2018-12-01

Large-Scale Testing of Low-Strength Cellular Concrete for Skewed Bridge Abutments

Rebecca Eileen Black
Brigham Young University

Large-Scale Testing of Low-Strength Cellular Concrete for Skewed Bridge Abutments

Rebecca Eileen Black

A thesis submitted to the faculty of
Brigham Young University
in partial fulfillment of the requirements for the degree of

Master of Science

Kyle M. Rollins, Chair
Norman L. Jones
Fernando S. Fonseca

Department of Civil and Environmental Engineering

Brigham Young University

ABSTRACT

Large-Scale Testing of Low-Strength Cellular
Concrete for Skewed Bridge Abutments

Rebecca Eileen Black
Department of Civil and Environmental Engineering, BYU
Master of Science

Low-strength cellular concrete is a type of controlled low-strength material (CLSM) which is increasingly being used for various modern construction applications. Benefits of the material include its ease of placement due to the ability of cellular concrete to self-level and self-compact. It is also extremely lightweight compared to traditional concrete, enabling the concrete to be used in fill applications as a compacted soil would customarily be used. Testing of this material is not extensive, especially in the form of large-scale tests. Additionally, effects of skew on passive force resistance help to understand performance of a material when it is used in an application where skew is present.

Two passive force-deflection tests were conducted in the structures lab of Brigham Young University. A 4-ft x 4-ft x 12-ft framed box was built with a steel reaction frame on one end a 120-kip capacity actuator on the other. For the first test a non-skewed concrete block, referred to as the backwall, was placed in the test box in front of the actuator. For the second test a backwall with a 30° skew angle was used. To evaluate the large-scale test a grid was painted on the concrete surface and each point was surveyed before and after testing. The large-scale sample was compressed a distance of approximately three inches, providing a clear surface failure in the sample. The actuator provided data on the load applied, enabling the creation of the passive force-deflection curves. Several concrete cylinders were cast with the same material at the time of pouring for each test and tested periodically to observed strength increase.

The cellular concrete for the 0° skew test had an average wet density of 29 pounds per cubic foot and a 28-day compressive strength of 120 pounds per square inch. The cellular concrete for the 30° skew test had an average wet density of 31 pounds per cubic foot and a 28-day compressive strength of 132 pounds per square inch. It was observed from the passive force deflection curves of the two tests that skew decreased the peak passive resistance by 29%, from 52.1 kips to 37 kips. Various methods were used to predict the peak passive resistance and compared with observed behavior to verify the validity of each method.

Keywords: abutment, backfill, cellular concrete, controlled low-strength material, lateral resistance, passive force, passive pressure

ACKNOWLEDGEMENTS

I would like to thank all those who have helped and supported me throughout graduate school and the thesis writing process. I thank all of the Civil Engineering faculty of BYU for their dedication to their students and their efforts to ensure that we are provided with skills to become not only successful engineers but also individuals with high character. I especially thank the members of my graduate advisory committee. I thank Kyle R. Rollins for allowing me to work on this project and for his dedication to his research and his students which I find inspiring. I thank Norm L. Jones and Fernando S. Fonseca for their willingness to revise and edit my work.

I would also like to express gratitude for all of my fellow students who participated in this research. Daniel Schwicht was not only vital to the completion of this research but also made the experience enjoyable through friendship. Pat Crummett, Megan Peffer, and Alex Temus all helped with the organization and implementation of this research. The faculty of the BYU Structures lab, Dave Anderson and Rodney Mayo, deserve the highest praise and gratitude for their help with this project. Their organizational skills and problem solving abilities made this research possible.

Funding for this study was provided by Federal Highway Administration (FHWA) pooled fund TPF-5(264) supported by the departments of transportation from the states of California, Minnesota, Montana, New York, Oregon, Utah, and Wisconsin. Utah served as the lead agency with David Stevens as the project manager. This support is gratefully acknowledged. I also express appreciation to Cell-Crete Corporation for the donation of cellular concrete material for this study.

TABLE OF CONTENTS

LIST OF TABLES

LIST OF FIGURES

1 INTRODUCTION

Lightweight cellular concrete (LCC) is a material which is increasingly being considered by contractors and designers as a replacement for traditional granular backfill adjacent to bridge abutments. Advantages to using LCC include its easy and rapid placement, reduced settlement of underlying soil, and reduced active earth pressures on the abutment wall. These are attributes which are especially important when the backfill passes over utility lines that are sensitive to settlement. LCC can be considered a controlled low-strength material (CLSM), however, by definition lightweight cellular concrete must have an oven dry density of 50 pounds per cubic foot or less. CLSM does not have this stipulation, therefore, not all CLSM is also LCC. Many of the material properties of LCC fall somewhere between conventional aggregate backfill and structural concrete. Because LCC doesn't fit neatly into a geotechnical or structural material category, large-scale testing is highly valuable in understanding its mechanical properties and basic behavior.

1.1 Research Objectives

The research objectives for this project were as follows:

1. Determine the ultimate passive force provided by lightweight cellular concrete.
2. Determine passive force-displacement relationships for cellular concrete backfill and the displacement necessary to mobilize ultimate passive force.
3. Compare available methods for predicting passive resistance with measured resistance.

4. Determine the skew angle effect on the passive resistance of cellular concrete backfill.

1.2 Scope of Work

To accomplish these objectives, two passive force-deflection tests were conducted in the structures lab of Brigham Young University. A 4-ft x 4-ft x 12-ft framed box was built with a reaction frame on one end and a 120-kip capacity hydraulic actuator on the other. For the first test, a non-skewed concrete block referred to as the backwall was placed in the box, and cellular concrete was poured in one 3-ft lift. For the second test, a concrete block with a 30° skew angle was used. Flow diameter, temperature, and air content were measured periodically throughout the concrete pour. Cylinders cast at pouring were tested at approximately 7 days, 14 days, 21 days, and 28 days to obtain data on the unconfined compression strength of the cellular concrete with time after placement.

After concrete placement, a grid was painted on the concrete surface after a period of curing and each point was surveyed with both a total station and auto level. String potentiometers were also installed at one to two-foot increments along the backfill to more accurately measure the longitudinal displacement of the cellular concrete. After the LCC cured for 7 to 10 days, an actuator was used to compress the cellular concrete. The test results allowed determination of the passive force-deflection relationship for each skew angle. Cracking patterns were noted and the grid points were re-surveyed. A comparison between the measured passive force with the 0° and 30° skew tests made it possible to evaluate potential reductions in resistance with skew angle and to compare this behavior with the behavior of conventional granular materials.

Finally, analyses were performed to predict the measured passive force-deflection curves using basic material parameters as proposed by various researchers. The analysis allowed researchers to determine which approaches can be reliably used to predict actual performance of a large-scale test and if modifications to proposed approaches should be made. However, the analyses were only performed on four separate cellular concrete tests and therefore cannot yet be extrapolated to cellular concrete in general. While these findings give evidence to which prediction method is most reliable for the two tests performed in this study as well as two previous large-scale cellular concrete tests, further testing is needed to determine if the results are generally applicable to the material.

1.3 Outline of Report

This thesis contains seven chapters. Chapter 1 contains the research objectives and scope of the testing that was performed. In Chapter 2 background information on cellular concrete, passive force theories, and relationships concerning bridge abutments and skew effects is provided. In Chapter 3 an overview of the test layout and instrumentation, as well as the data analysis methods is given. In Chapter 4 information is provided on cellular concrete properties observed throughout the testing. In Chapter 5 the passive force test results are detailed, while in Chapter 6 an analysis of the results is given. Chapter 7 contains conclusions and recommendations based on the findings of the tests.

2 LITERATURE REVIEW

2.1 Low-Strength Cellular Concrete

Cellular concrete is a variety of concrete that differs from the traditional concrete components of cement, aggregates and water. Instead, it consists of an aerated cement slurry which is easily pumped and flowable enough to be self-leveling. According to ACI 523, cellular concrete is "concrete made with hydraulic cement, water, and preformed foam to produce a hardened material with an oven dry density of 50 pounds per cubic foot or less" (ACI Committee 523 2006). Because of this qualification, controlled low-strength material (CLSM) cannot always be classified as cellular concrete because it may have a density higher than 50 pounds per cubic foot. However, cellular concrete can be classified as CLSM.

The foam for cellular concrete is created with a liquid foam concentrate which is diluted with water and passed through a foam generator (Sutmoller 2017). Cellular concrete contains 50-80% more air voids than typical concrete (Grutzeck 2005), and its compressive strength is significantly lower than that of traditional concrete.

Applications for this product include reducing active earth pressures, mitigating settlement, and absorbing earthquake forces in subsurface structures (Tiwari et al., 2017). Cellular concrete has also been used in projects throughout the United States for soft soil remediation in areas such as New Orleans and the Pacific Northwest (Sutmoller 2017). Its quick and easy installation process and ability to be pumped into hard-to-reach locations also makes it a desirable option for

construction (Taylor 2014). Another advantage to using cellular concrete is that this material is easy to excavate. Unlike traditional concrete, cellular concrete may be excavated with a backhoe, if necessary.

2.2 Physical Characteristics of Low-Strength Cellular Concrete

2.2.1 Unit Weight

Caltrans has developed a schedule of cellular concrete classes based on the unit weight of the concrete. It ranges from I to VI and encompasses cast densities of 24 lb/ft^3 to 90 lb/ft^3. The compressive strength associated with the classes varies from 10 to 300 psi, as shown in Table 2-1. This can be used for specifying concrete density to achieve a specific strength for a given application. For the purposes of this study cellular concrete generally falling into the class of II was used. However, this table demonstrates the higher strengths that can be achieved by using cellular concrete of a higher cast density. Classes I through IV are most commonly used in practice (Remund 2017).

Table 2-1: Caltrans Cellular Concrete Classes (Remund 2017)

Cellular Concrete Class	Cast Density (lb/ft^3)	Minimum 28-day Compressive Strength (psi)
I	24-29	10
II	30-35	40
III	36-41	80
IV	42-49	120
V	50-79	160
VI	80-90	300

2.2.2 Unconfined Compressive Strength

Cellular concrete has a much lower unconfined compressive strength than other concretes. Table 2-2 provides typical guidelines for cellular concrete mixes, including the typical compressive strength at 28 days for cellular concrete at various cast densities. As with other concrete mixes, strength increases with higher cast density. However, unlike traditional concrete, low strength cellular concrete does not exhibit brittle failure after reaching its peak compressive strength. Figure 2-1 shows the ductile behavior of cellular concrete at lower cast densities. More brittle behavior is observed in samples with a higher cast density.

Table 2-2: Typical Guidelines Cellular Concrete Mixes (Sutmoller 2017)

Cast Density		Typical Compressive Strength at 28 days		Portland Cement		Water		Foam Volume	
lb/ft³	kg/m³	psi	MPa	lb/yd³	kg/m³	gal	L	ft³/yd³	m³/m³
20	320	50	0.34	328	195	19.7	97.3	22.7	0.84
25	400	80	0.55	420	249	25.2	124.6	21.5	0.80
30	481	140	0.97	512	304	30.7	151.9	20.3	0.75
35	561	210	1.45	603	358	36.2	178.8	19.1	0.71
40	641	330	2.28	695	412	41.7	206.1	17.9	0.66
45	721	450	3.10	787	467	47.2	233.4	16.7	0.62
50	801	640	4.41	878	521	52.6	260.4	15.5	0.57
55	881	790	5.45	970	575	58.2	287.7	14.3	0.53
60	961	930	6.41	1062	630	63.7	315.0	13.1	0.49

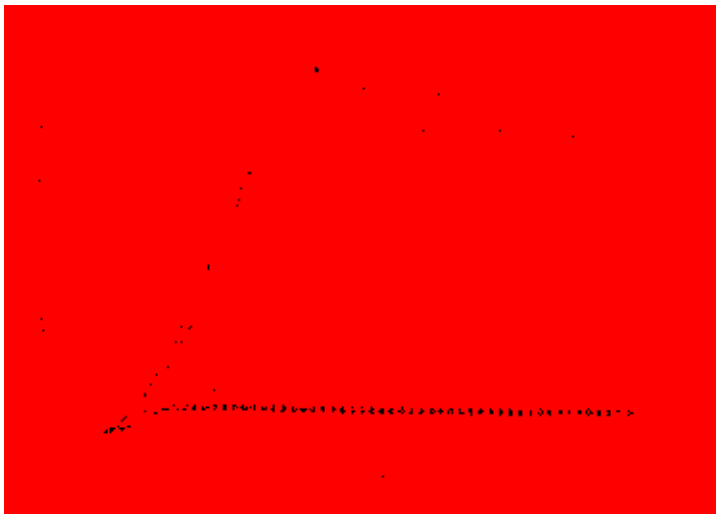

Figure 2-1: Stress-strain curves from the UC test (Tiwari et al. 2017)

A strong correlation has been shown between unconfined compressive strength and the unit weight of the concrete. Figure 2-2 shows the result from Tiwari et al. (2017). The data presented in this figure shows a majority of the unconfined compressive strengths falling within the bounds of ± 0.5 standard deviations of the best-fit regression line. However, because of the difficulty in producing a large batch of cellular concrete with a specific unit weight without variation, it is significant to note that there may be substantial scatter about the mean unconfined compressive strength of the sample if the unit weight is not consistent. For the purposes of this study the unit weight remained fairly consistent, and had a target density of approximately 30 pounds per cubic foot. A discussion of the properties of cellular concrete with substantially different unit weight values is beyond the scope of this project. It should be noted that further research could be done on the effects observed if a cellular concrete with a much higher unit weight is used.

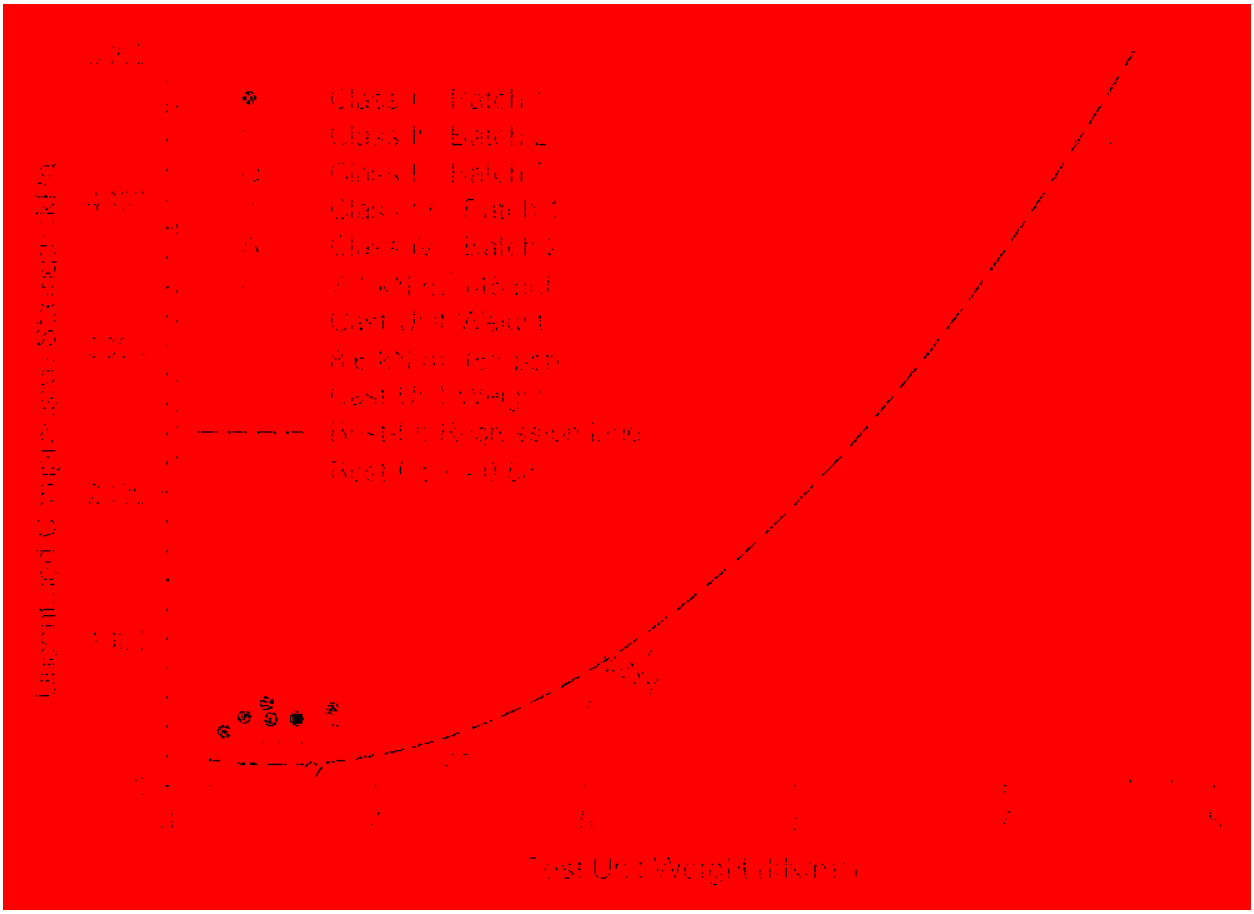

Figure 2-2: Relationship between unconfined compressive strength of LCC specimens with their corresponding test unit wights (Tiwari et al. 2017).

2.2.3 Shear Strength

A proposed way of measuring the shear strength of deep-mixed soil-cement is with Mohr's circle and a cohesion value estimated as 0.7 times 50% of the unconfined compressive strength (Filz, et al. 2015). This indicates that 50% of the unconfined compressive strength accounts for the shear strength of the material, while the 0.7 factor is a reduction given to a small sample (Filz, et al. 2015). The direct tension Mohr's circle is equal to 0.12 times the unconfined compressive strength as shown in Figure 2-3 (Filz, et al. 2015). The strength envelope is taken as the highest shear strength based on the unconfined compression Mohr's circle and following along the unconfined compression Mohr's circle until reaching a line tangent to the direct tension Mohr's

circle, as shown in Figure 2-3. This process assumes a friction angle of 0°. This proposed method was also used in an analysis of controlled low-strength material by Wagstaff (2015), and in an analysis of cellular concrete by Remund (2017).

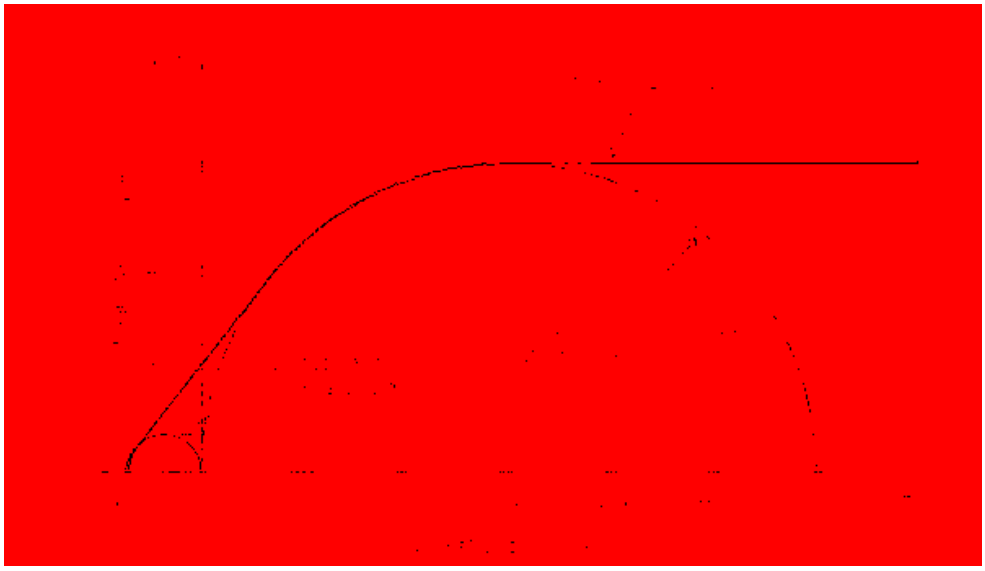

Figure 2-3: Proposed example strength envelope for deep-mixed soil-cement including tension (Filz, et al. 2015).

2.2.4 Cohesion and Friction Angle

Several methods have been proposed to evaluate cohesion and friction angle of cellular concrete. Tiwari et al. (2017) proposed the following equations:

$$\varphi = 1.187\,\gamma + 15.062 \qquad \text{Equation 2-1}$$

$$c = 274.386\,\gamma - 654.958 \qquad \text{Equation 2-2}$$

where:

φ = Friction angle

c = cohesion

γ = wet density of cellular concrete backfill (kN/m^3)

Tiwari et al. (2017) also proposed from a direct simple shear test of the Class-II cellular concrete that the friction angle was 35° with a cohesion intercept equal to 36 kPa. Through studying behavior of Class-II and Class-IV cellular concrete, Tiwari et al. (2017) found that the LCC exhibited an effective friction angle of 34° and a cohesion intercept of 78 kPa. Studies performed by Remund (2017) and Wagstaff (2016) used a friction angle of 0° and a cohesion value equal to half of the unconfined compressive strength. It is unclear which of the methods for determining friction angle and cohesion are the most accurate.

2.2.5 Advantages of Cellular Concrete

Cellular concrete exhibits many features which are advantageous for certain applications. Cellular concrete is flowable and can be pumped directly into locations that may be hard to reach with other methods (Taylor 2014). Cellular concrete is self-leveling and self-consolidating. This saves time and money in labor and machine costs which are necessary when compacting soil as may be done as an alternative to cellular concrete. Another advantage is that cellular concrete is excavatable with a backhoe. This can be extremely beneficial if it is above utility lines that may need to have maintenance work performed on them.

Cellular concrete has a low unit weight compared to traditional concrete. This is both an advantage and a disadvantage, depending on the use. For uses such as reducing earth pressures, mitigating settlement, and absorbing earthquake forces in subsurface structures (Tiwari, Ajmera and Maw, et al. 2017), the low unit weight and correlating lower strength is not an issue. It is an advantage because cellular concrete, unlike traditional concrete, can be used for fills over soft compressible soil, particularly where settlement might damage sensitive utility lines (Sutmoller 2017). For example, if some of a heavier native soil is replaced with a new fill of cellular concrete

prior to construction, it will not induce any load. Additionally, cellular concrete has been used as a way to mitigate negative effects of earthquake ground movement around tunnels and pipelines (Tiwari, Ajmera and Villegas 2018). A potential way for cellular concrete to be used is as a backfill behind bridge abutments. This is a use which determined the set-up of this particular large-scale cellular concrete test.

2.2.6 Disadvantages of Cellular Concrete

As mentioned in the previous section, the low unit weight of cellular concrete and corresponding lower strength could be considered as a disadvantage for certain applications. Cellular concrete would not be suitable for many of the structural applications of traditional concrete. Another disadvantage of cellular concrete is the fact that it is not as well tested as traditional concrete. Although it has been in existence since the early 1900's, it is becoming increasingly common in recent years (Sutmoller 2017). This may help the material become more readily available at any given location, because at present there are some constraints as to where the material is easily accessible (Remund 2017). The cost of cellular concrete can also be considered a disadvantage. In some cases, the cost of materials is more expensive than other options, so advantages must be weighed in other categories for the material to be used. A final disadvantage of cellular concrete is availability of the material. A specialized contractor must be found which can perform the placement of the cellular concrete.

2.3 Passive Earth Pressure

2.3.1 Log-spiral Method

There are three commonly accepted and generally used passive earth pressure theories: Rankine, Coloumb, and Log-spiral. Tests performed by Mokwa and Duncan (2001), Rollins and Sparks (2002), and Rollins and Cole (2006), each suggested that the log-spiral method predicted the failure geometry with the most accuracy. The log-spiral method is the one which will be primarily discussed for cellular concrete backfills.

Figure 2-4 depicts a typical condition where passive earth pressures would exist. If there is a bridge with a bridge abutment and seismic activity causes the ground to move, the abutment will push into the soil, thereby mobilizing the passive pressure. The figure depicts the movement of the abutment in a dashed line and the directionality of the forces with the arrows. Bridge abutments are a significant topic of study, as they are an important part of the infrastructure of a city and can often be damaged through large seismic events. More information on this topic is discussed in Section 2.5

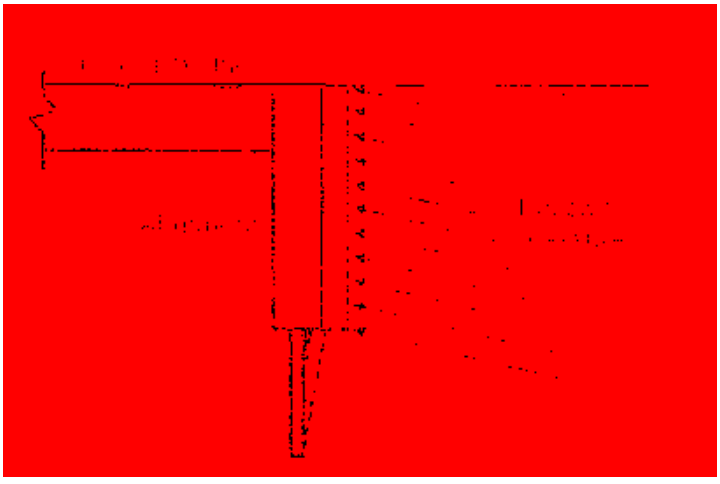

Figure 2-4: Abutment passive earth pressure illustration (Duncan and Mokwa 2001).

The log-spiral method differs from the other methods in its prediction of a failure surface with a log-spiral segment followed by a linear segment inclined at 45-φ/2 from the horizontal. This differs from the Rankine and Coulomb, which both assume a linear failure surface from the base of the wall to the ground surface inclined at 45-φ/2. As shown in Figure 2-5, the failure surface extends below the embedded wall before connecting with the surface. Both the log-spiral and the Coulomb methods require the use of a wall friction angle, which is typically between 0.65φ to 0.8φ for granular materials. A disadvantage to using the log-spiral method is the time and complication in equations which provide a graphical solution. The following section will address a strategy to facilitate efficiency in the use of the log-spiral method.

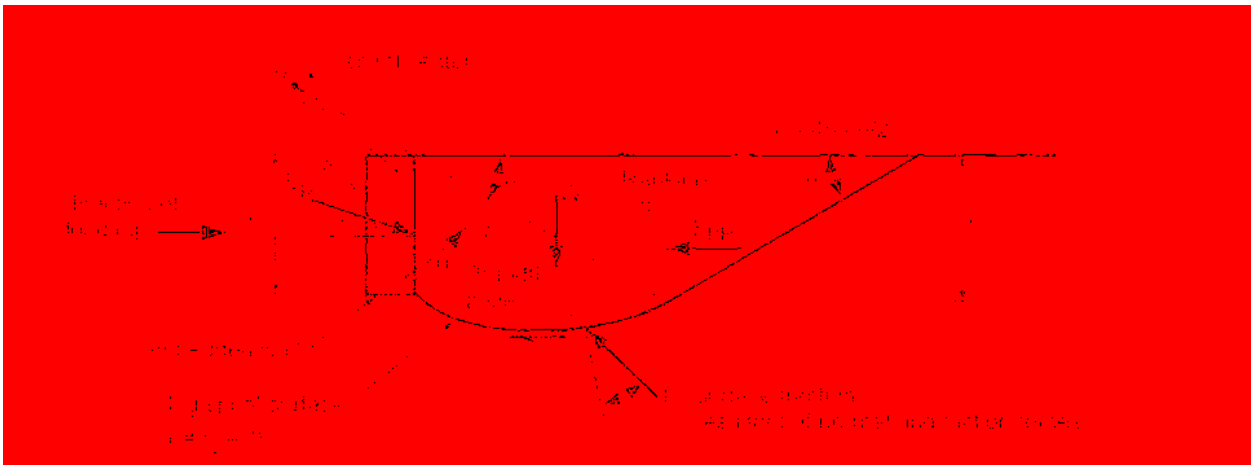

Figure 2-5: Log-spiral failure mechanism (Duncan and Mokwa 2001).

2.3.2 PYCAP as a Modeling Tool

In order to facilitate the use of the Log-spiral method to predict passive pressure and load deflection curves for pile caps, Mokwa, Duncan, and Via (2000) developed a coded excel spreadsheet called PYCAP. The calculations involved in using the log-spiral method can be tedious, however, with the use of this spreadsheet, a few parameters may be entered to generate

the results automatically. The parameters are: cap width, cap height, embedment depth, surcharge, cohesion, soil friction angle, wall friction, initial soil modulus, Poisson's ratio, soil unit weight, and adhesion factor. The program uses these parameters to calculate the passive force on the wall as well as develop a curve for the predicted failure surface. Figure 2-6 shows the input parameters and values that are generated automatically by the spreadsheet. Figure 2-7 depicts the failure surface and Figure 2-8 the hyperbolic model of cap deflection. PYCAP allows for these figures to be created efficiently and for the input values to be altered to view how some of the parameters which are only estimates may be altered to provide results from the program that more closely match results that are observed in the field.

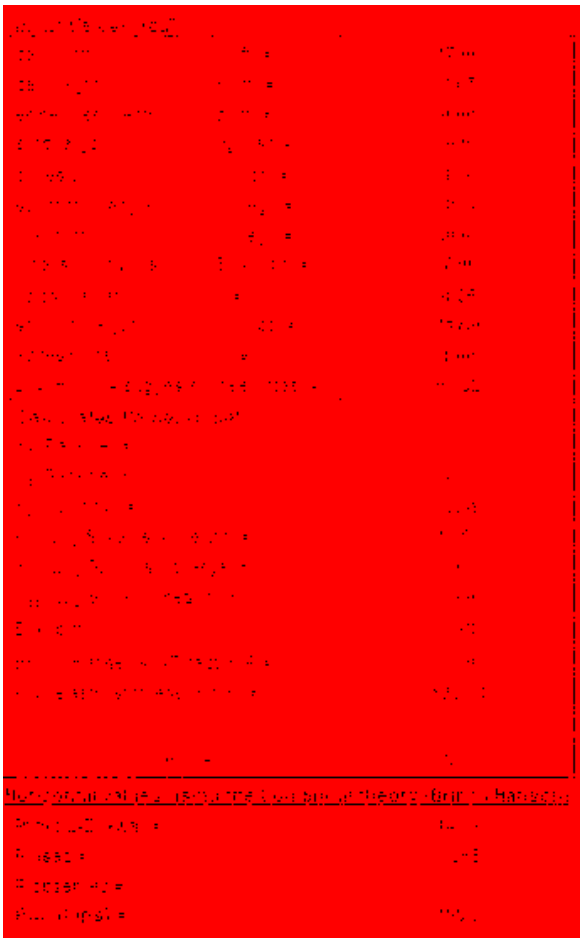

Figure 2-6: Input and calculated values from the PYCAP program.

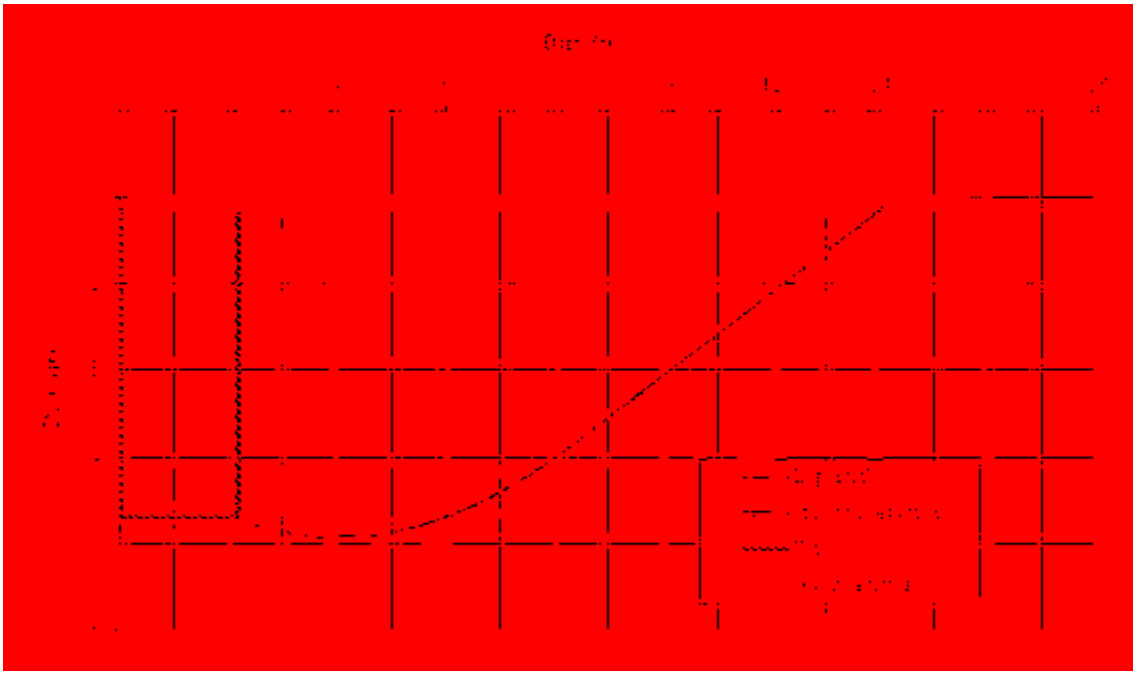

Figure 2-7: Log-spiral geometry generated by the PYCAP program.

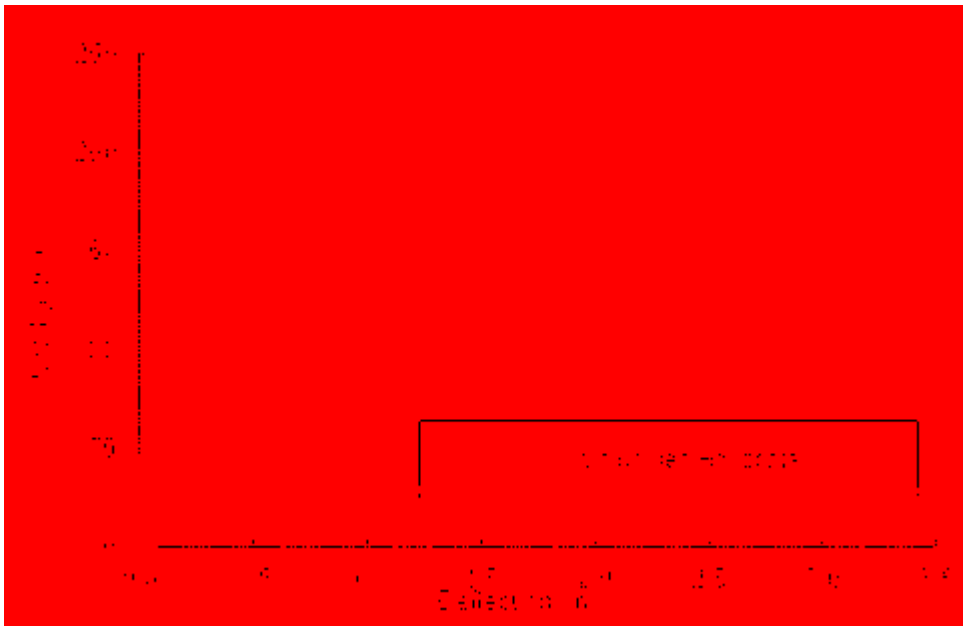

Figure 2-8: Hyperbolic model of cap deflectoin with PYCAP program.

2.4 Passive Force-Displacement Tests for Non-Skewed Abutment Walls

Many tests have been performed on passive force-displacement for various materials. The general curve observed follows a nearly hyperbolic path with a greater rate of increase at the beginning and a lower rate of increase as the curve approaches the ultimate passive force reached by the backfill material. The theoretical force vs. deflection curve is shown in Figure 2-9.

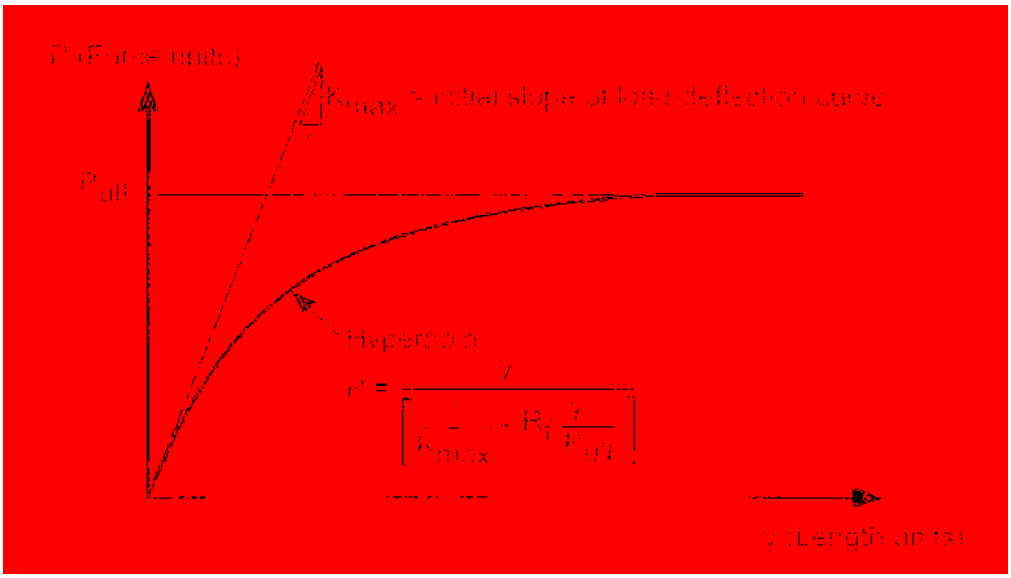

Figure 2-9: Hyperbolic load-deflection curve (Duncan and Mokwa 2001).

Data was compiled by Frederickson (2015) to determine at what point various materials reached peak deflection. She concluded from her study that all failed or nearly failed at deflections between approximately 2-5.5% of their respective wall heights. This is shown in Figure 2-10 and Figure 2-11. In two large-scale tests performed on cellular concrete by Remund (2017), peak passive force was reached at 1.7 and 2.6% of the wall height. This is on the lower end of the range of values obtained by Frederickson for granular materials.

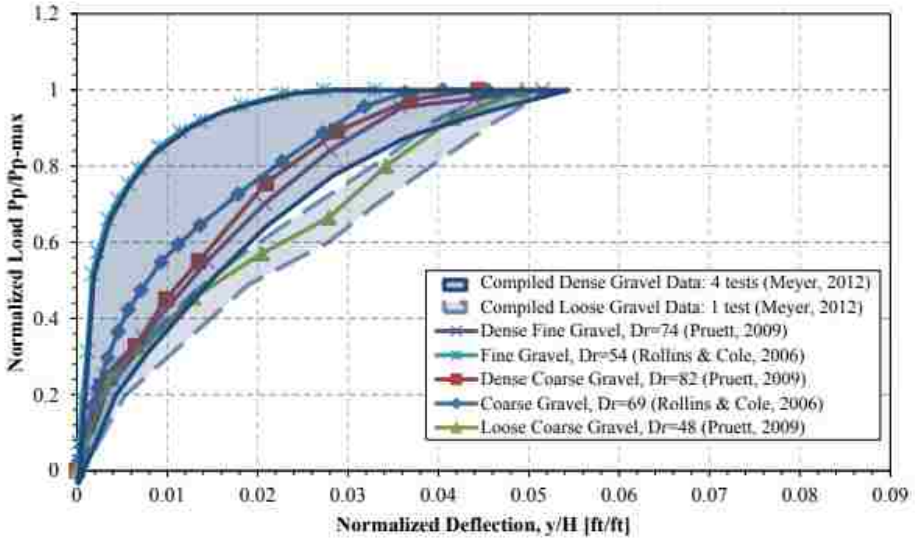

Figure 2-10: Compilation of passive force-deflection data for dense and loose gravels (Frederickson, 2015).

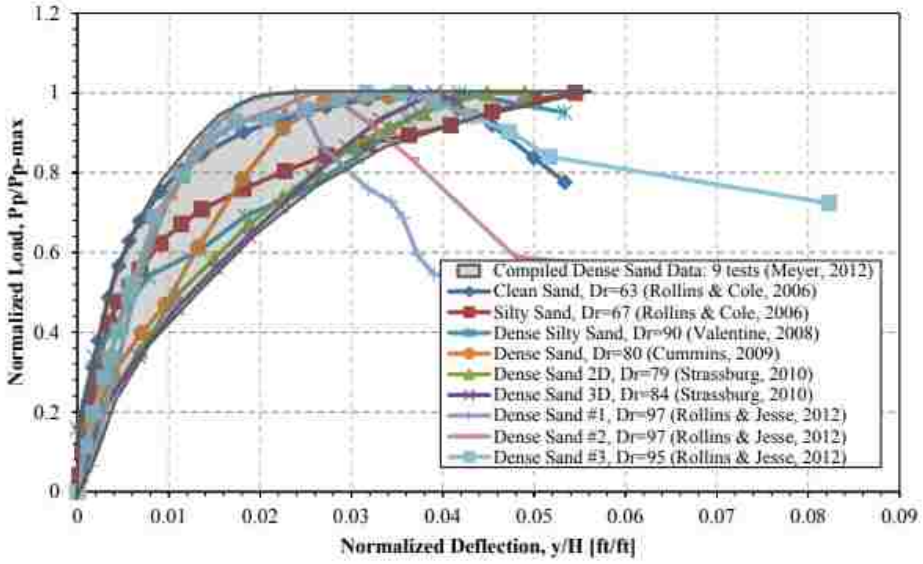

Figure 2-11: Compilation of passive force-deflection data for dense and loose sands (Frederickson, 2015).

2.5 Skewed Bridge Earthquake Performance

Studies of bridge failures have repeatedly shown that skew has an adverse effect on seismic performance (Shamsabadi, Rollins and Kapuskar 2007). In an earthquake event, the abutment is pushed into the earth, thus activating passive earth pressure. The movement of the bridge structure during the earthquake is highly dependent on the passive resistance that is developed at the bridge abutment. FHWA recommends minimizing skew to the extent possible, however they also acknowledge the fact that existing infrastructure may make this difficult or impossible (FHWA 2014). Therefore, it is extremely important that the effects of skew are studied and used in design.

2.6 Passive Force-Displacement Tests for Skewed Abutment Walls

Many tests have been performed to analyze the effect of skew on passive force. Figure 2-12 demonstrates the decrease in passive force observed by Marsh (2013) when tests were performed on an abutment with progressively higher skew angles with a backfill of dense, compacted sand. Figure 2-13 shows similar trends for a 75 ft wide bridge abutment with a sand backfill modeled with the 3D finite element program Plaxis (Shamsabadi, Kapuskar and Zand 2006). Figure 2-14 shows similar trends observed by Rollins and Jessee (2013) using a 4 ft wide by 2 ft high wall with four skew angles and a backfill material of clean compacted sand. In each case an increase in skew angle led to a decrease in passive force observed in the backfill material.

Rollins and Jessee (2013) proposed the use of a skew reduction factor (R_{skew}) to account for reduced passive resistance as a function of skew angle. The equation for R_{skew} was defined from available test data by Shamsabadi and Rollins (2014) for sand or gravel backfills.

$$\mathbf{R_{skew}} = \frac{P_{p-skew}}{P_{p-no\ skew}} = e^{\left(\frac{-\theta}{45^\circ}\right)} \qquad \text{Equation 2-3}$$

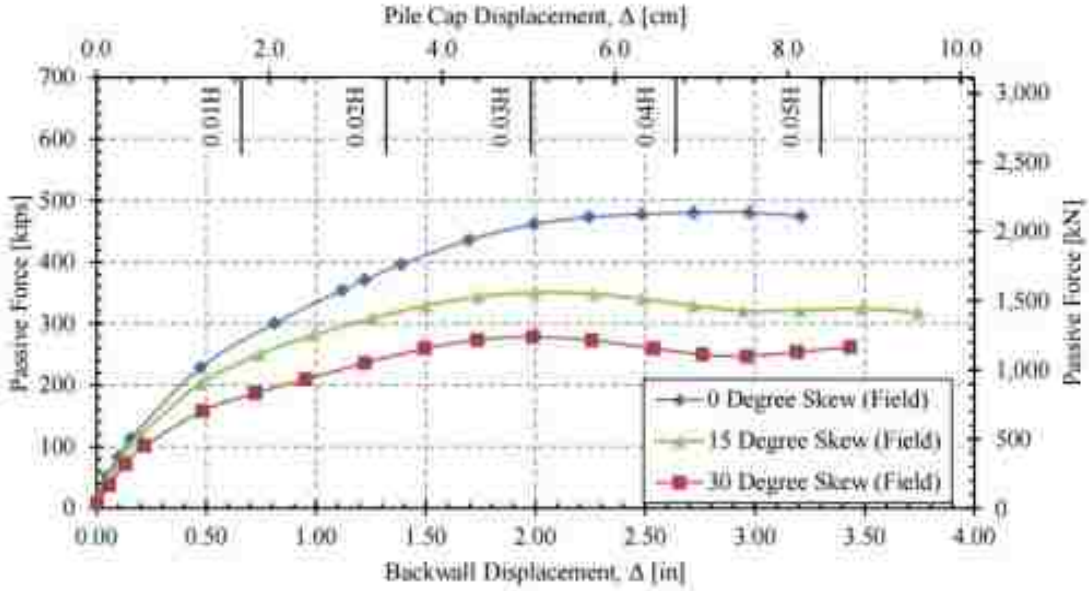

Figure 2-12: Passive force-deflection curves for the 0°, 15°, and 30° tests (Marsh, 2013).

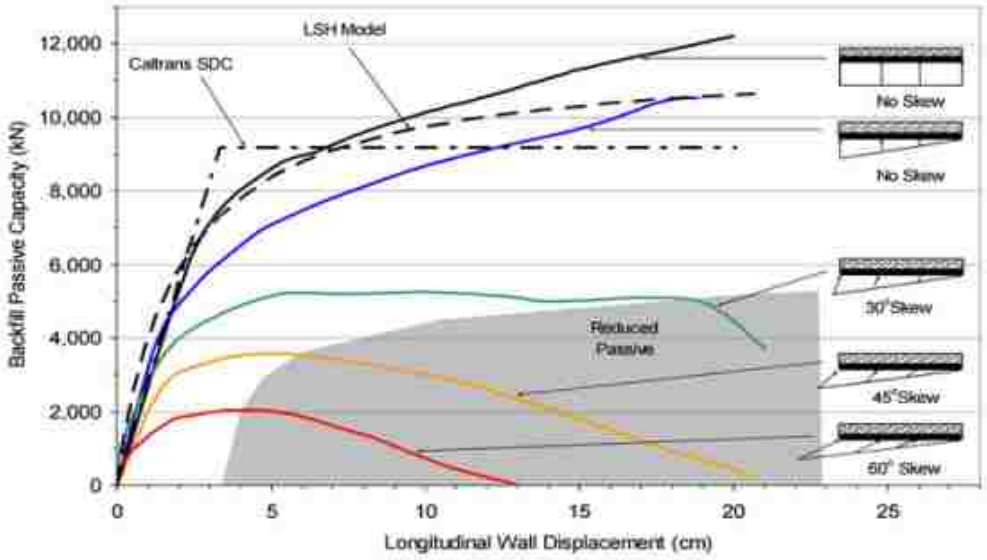

Figure 2-13: Passive force-deflection curves for 0, 30, 45, and 60° skew angles (Shamsabadi, Kapuskar and Zand 2006)

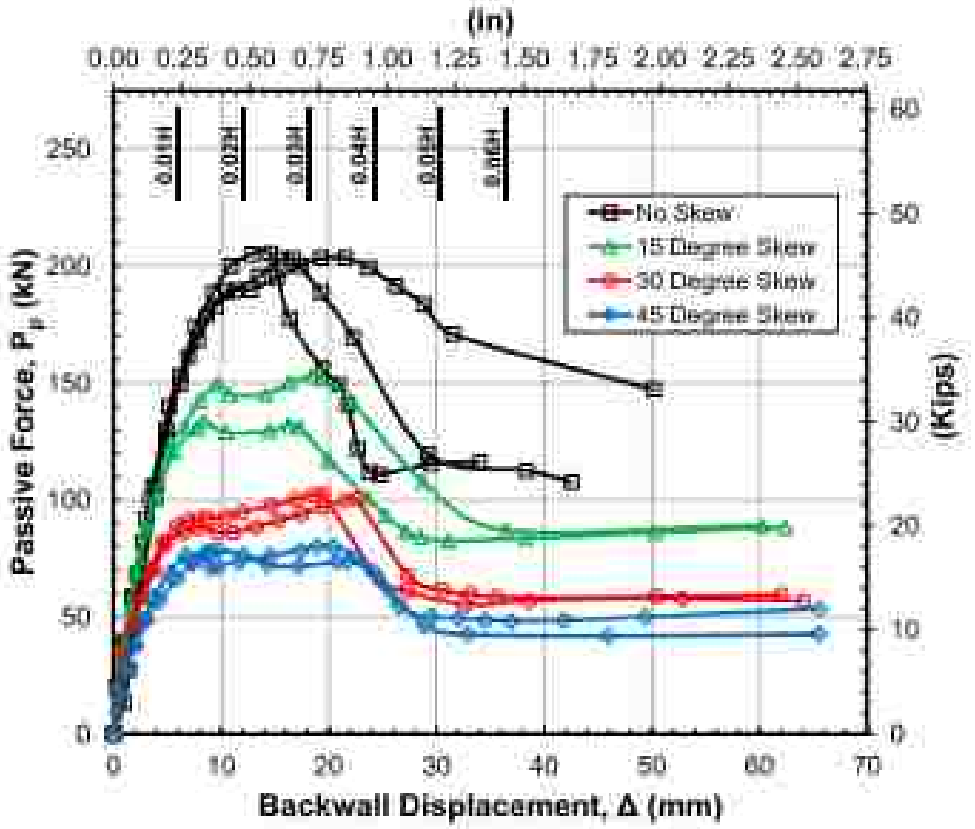

Figure 2-14: Passive force versus longitudinal deflection curves at various skew angles (Rollins and Jessee 2013).

Two exceptions to these findings regarding the effect of skew angle were observed by Remund (2017), and Wagstaff (2016), in large-scale tests of cellular concrete and controlled low-strength material, respectively. As shown in Figure 2-15, peak passive force increased for the 30° skew test. While there were other factors that could have had an influence on the passive resistance such as a higher unit weight of concrete on the 30° test, it should still be noted that the decrease in passive force was not observed in this test. Similarly, in Figure 2-16, the 30° skew test has a higher passive force.

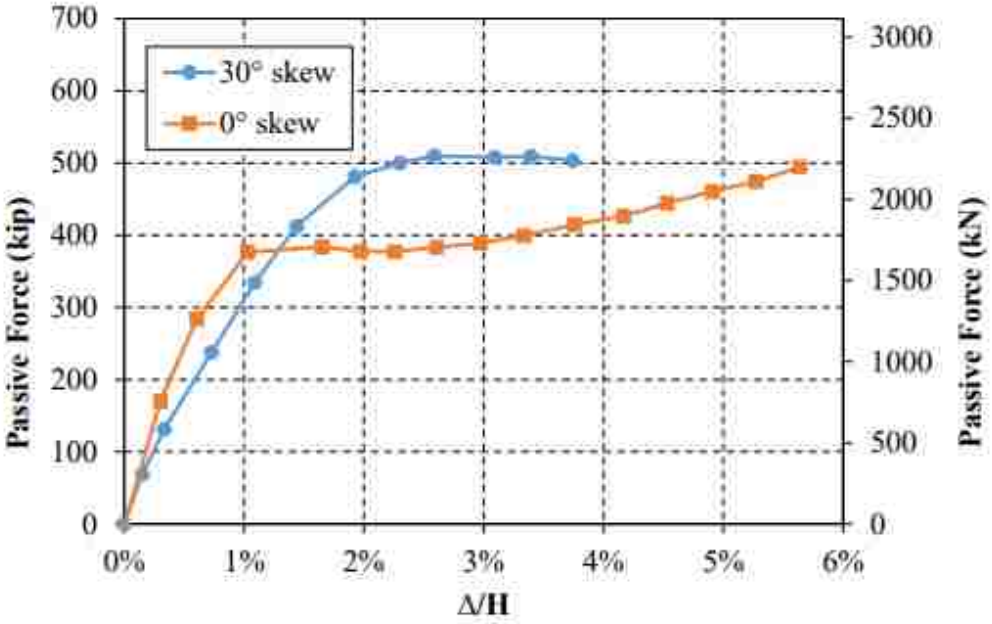

Figure 2-15: Passive force vs. normalized displacement for 30° and 0° skew cellular concrete field tests (Remund 2017).

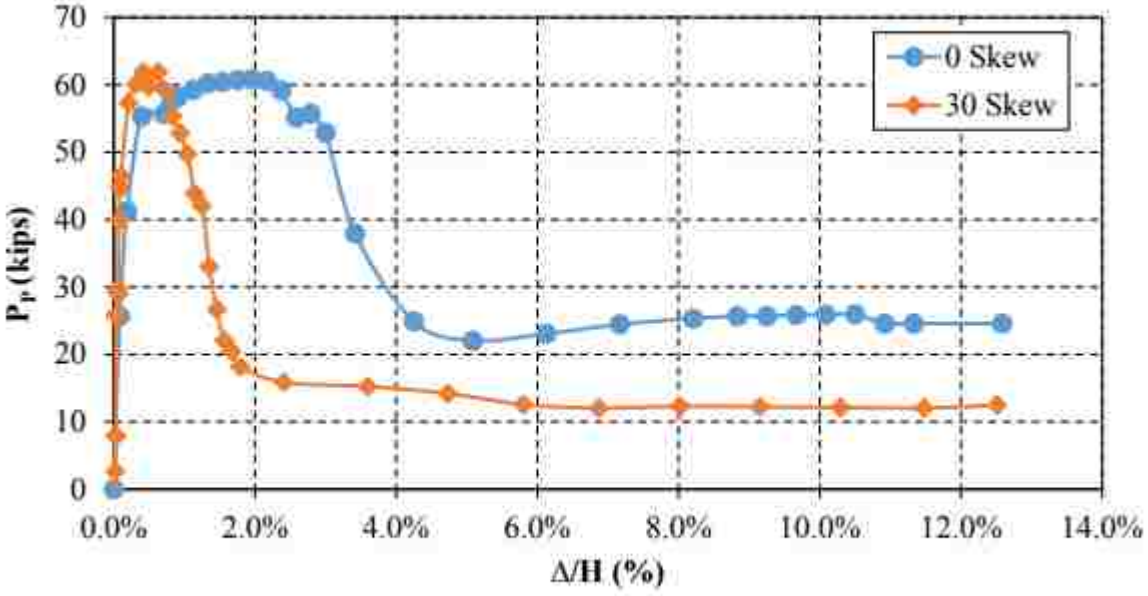

Figure 4-4. Passive force versus normalized displacement.

Figure 2-16: Longitudinal load versus normalized displacement for 0° and 30° skew CLSM backfill (Wagstaff, 2016).

2.7 Literature Review Summary

Cellular concrete is a material well worth investigating. It is becoming increasingly used in construction applications and has been shown to be advantageous for uses in soft soil remediation, reducing active earth pressures, mitigating settlement, and absorbing earthquake forces. Cellular concrete is self-leveling and self-consolidating and has a unit weight from 24 pounds per cubic foot to 90 pounds per cubic foot. Its compressive strength at 28 days ranges from 50-930 pounds per square inch. While the material does exhibit shrinkage, there are ways to mitigate negative effects caused by this.

Various tests have been performed to evaluate passive earth pressures. It has been shown that the log-spiral method is the most accurate for predicting the failure surface of laterally loaded pile caps (Remund 2017). PYCAP is a program that has been developed to aid in the prediction of passive force vs. deflection curves, as well as peak passive resistance and failure geometry. Skew has been shown to decrease the peak passive resistance exhibited by materials. Peak passive pressure has been shown to be reached between 2-5.5% of backwall height for both cohesive and non-cohesive soils. This value has been shown to be slightly lower for cellular concrete, however repeated testing will be valuable to verify the validity of this assumption. This study will explore the relationship between skew and passive force when cellular concrete is used as the backfill adjacent to bridge abutments.

One uncertainty that exists with cellular concrete is whether it should be treated as a cohesive material with cohesion equal to half of the unconfined compressive strength and friction angle equal to zero or if the friction angle should be taken as 34-35 degrees with a minimal cohesion. This is a topic that needs further research and analysis.

3 TEST LAYOUT, INSTRUMENTATION, AND TEST PROCEDURE

3.1 Overview

All tests were performed in the structures lab of Brigham Young University in Provo, UT. A view of the test configuration is shown in Figure 3-1. A combination of concrete blocks, plywood, plastic sheeting, and steel reaction frames were used as shown to create the test box used for the two passive force tests with skew angles of 0° and 30°. Cellular concrete was placed inside the box and load was applied with a 120-kip actuator. Measurements were made of backfill heave and horizontal displacement, along with ultimate failure geometry. Data from a variety of instrumentation was captured with a data acquisition system and stored for subsequent analysis.

Figure 3-1: Photo of 0° skew test box layout before placement of LCC backfill.

3.2 Test Layout

Two passive force-deflection tests were conducted with LCC backfill in the structures lab of Brigham Young University. A 4-ft x 4-ft x 12-ft framed box was built with a steel reaction frame on one end and a 120-kip capacity actuator on the other, as shown in Figure 3-2. For the first test a non-skewed concrete block, referred to as the backwall, was placed in the test box in front of the actuator. For the second test a backwall with a 30° skew angle was used as shown in Figure 3-3. In each instance the backwall was placed on 1 ¼" ø steel roller to avoid friction between the base of the backwall and the underlying wooden support platform. This arrangement is shown in Figure 3-4.

Figure 3-2: Photo of 0° skew test box layout without plastic sheeting.

Figure 3-3: Photo of 30° skew test box layout before LCC backfill.

Figure 3-4: Photo of 0° skew test roller bar below base of backwall to reduce base friction.

The cellular concrete was poured into the test box in one 3-ft lift. A 6-in grid was painted on the concrete surface and each point was surveyed with both a total station and auto level before and after testing to document heave and lateral displacement. The grid was also valuable in locating the eventual failure surface geometry. String potentiometers were also installed at 2 ft increments to more accurately measure the longitudinal displacement of the cellular concrete backfill with distance from the backwall.

3.3 Instrumentation

3.3.1 Longitudinal Load Instrumentation

The MTS actuator used for the passive force test is manufactured with pressure transducers which provide information about the load applied to the backwall from the actuator. A continuous measurement of the actuator load was obtained with a data acquisition system. The actuator was mounted to the center of the backwall.

3.3.2 Backfill Surface Heave

To monitor the surface heave and lateral displacement of the cellular concrete backfill during loading, a 6-in grid was spray painted on the backfill surface as shown in Figure 3-5 and Figure 3-6. The grid was surveyed with both an auto level accurate to 0.001 ft and a total station before and after the testing to gather data on the movement of the cellular concrete backfill. The grid was painted on the cellular concrete after a period of curing of at least 48 hours. This was to ensure that the concrete had hardened sufficiently for the surface to be walked on without damage to the surface of the concrete.

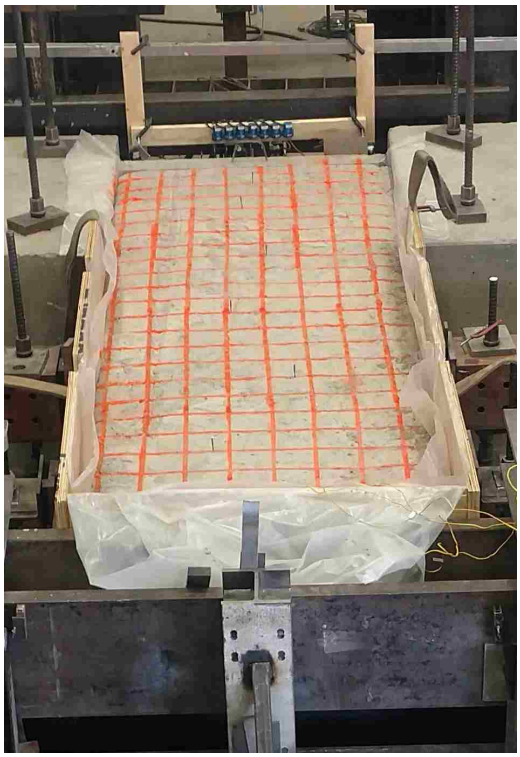

Figure 3-5: Photo of 0° skew backfill grid prior to loading.

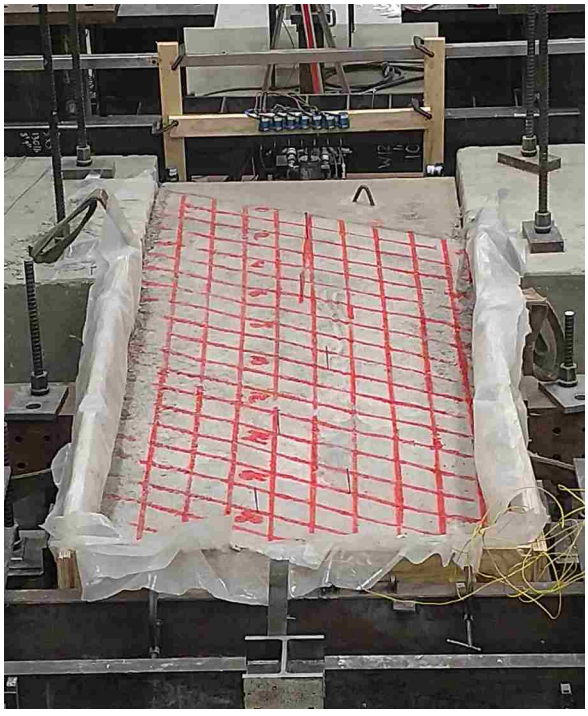

Figure 3-6: Photo of 30° skew backfill grid prior to loading.

3.3.3 Longitudinal Displacement Instrumentation

To measure the movement of the backwall and reaction frame, nine string potentiometers were placed at a height of 3 to 6 in at various locations and monitored for movement throughout the test. Four were placed at various locations on the reaction frame itself, four on the backwall, and one on the steel frame above the backwall. Figure 3-7 shows a plan view of the test layout for the 0° skew test and corresponding locations of string potentiometers. These locations were chosen to ensure that the test box and reaction frame did not significantly move, thereby affecting the results of the test. It is noted that although the figure shows the string potentiometer locations for the 0° skew test, the instrumentation layout was the same for the 30° skew test as well.

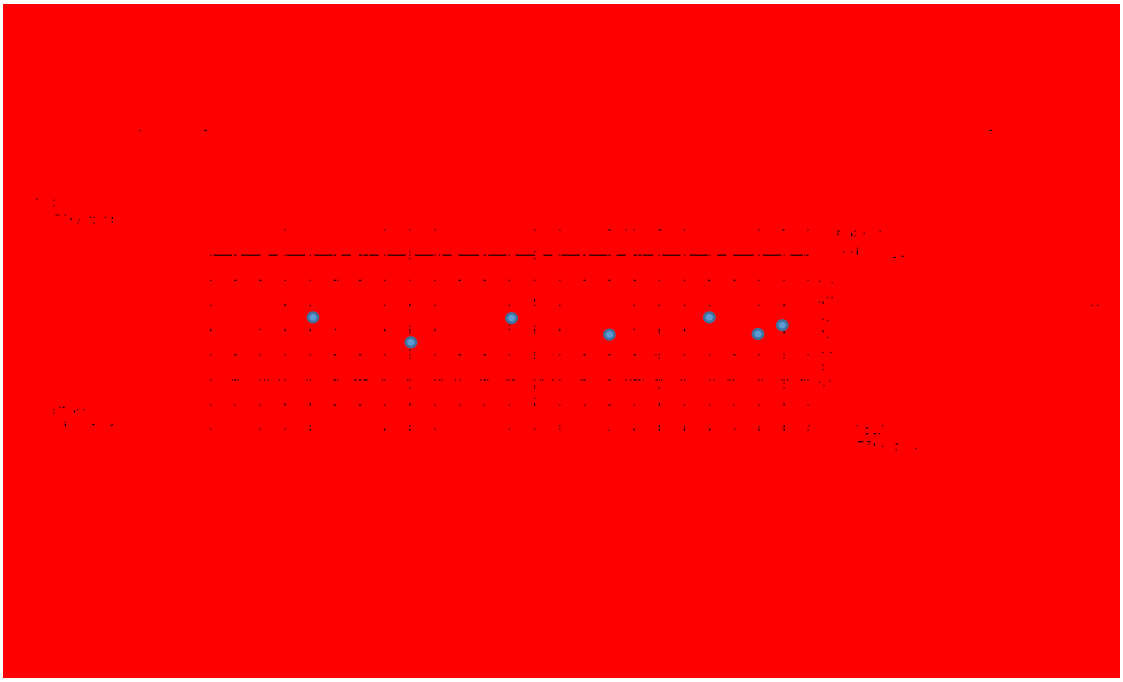

Figure 3-7 : Plan view of longitudinal displacement string potentiometer locations.

3.3.4 Backfill Compressive Strain Instrumentation

String potentiometers were also used to gather data on the backfill displacement. String pots were connected to screws embedded in the surface of the cellular concrete at approximately 2-ft intervals as shown Figure 3-7 of the previous section. These were then attached to an independent reference frame as shown in Figure 3-8. The string potentiometers were used, in addition to surveying the grid points, to provide a continuous recording of horizontal backfill movement throughout the duration of the test instead of merely at the beginning and end. Incremental backfill compressive strain and overall backfill movement could be computed from the difference in movement between adjacent points.

Figure 3-8 : String potentiometers mounted on independent wooden reference frame to monitor longitudinal deflection of the LCC backfill surface.

3.3.5 Thermocouple Instrumentation

Three thermocouple lead wires were placed approximately 6 in. from the back wall of the test box at heights of 6 in., 18 in., and 27 in. from the top of the fill. A fourth thermocouple lead wire was placed directly into an LCC test cylinder and placed in a cooler next to the test box to ensure that it was not disturbed. These thermocouples were used to monitor the curing temperatures of the LCC at different depths in the backfill as well as that of the test cylinders that were cast for UCS testing.

3.4 Testing Procedure

3.4.1 Cellular Concrete Placement and Testing

The cellular concrete for this test was provided by Cell-Crete Corporation. It was mixed by a concrete mix truck and pumped directly into the test box. The cellular concrete was placed in one 3-ft (0.91-m) lift as per Caltrans specifications. Samples were taken periodically to ensure that the concrete density remained around the target density of 27 pounds per cubic foot. A 4-in x 8-in plastic cylinder was filled with cement slurry and weighed to obtain the wet density. Adjustments in the foam content could then be made by truck operators to adjust the density of the cellular concrete. Samples for Unconfined Compressive Strength testing were taken in the middle of pump flow and placed in Styrofoam cubes with (4) 3-in x 6-in cylinders. These cylinders were used for UCS testing as discussed in Section 4.2.1. Air content and flowability of the cellular concrete were also measured as discussed in Section 4.2.2 and Section 4.2.3.

3.4.2 Loading Procedure

To apply a horizontal force to the cellular concrete fill, a 120 kip (490 kN) actuator was bolted to the 0° backwall and the 30° backwall. The actuator displaced the blocks longitudinally at a rate of 0.1 in/min (0.25 cm/min) until a displacement of approximately 3 in. (76.2 mm) was reached. This deflection is equal to 12.5% of the height of the backwall (H) while full passive force was expected to develop at approximately 3% of H. By this displacement a clear failure surface had developed in the cellular concrete fill and a complete record of passive force-deflection could be observed. Post-peak passive force-displacement behavior is significant for assessing whether the failure of the LCC is brittle or ductile in nature. For seismic loading conditions, a ductile failure is preferable and has been observed in previous LCC tests performed by Remund (2017).

4 CELLULAR CONCRETE PROPERTIES

4.1 Mixture Design

For the 0° and 30° skew tests, a slurry with a water cement ratio of 0.55 was used and foam was added to achieve the target density of around 27 pounds per cubic foot. The mix design details are shown in Table 4-1.

Table 4-1: Cellular Concrete Mixture Design

Mix Design Designation:	CCC 27-55
Cast Density (pcf):	27.00
Water/Cement Ratio:	0.55
Foam Type & Lot #:	JLE
Foam/Air Volume:	1.05
Foam Density (pcf):	3.5
Foam Rate (cfm):	32.00
Quantity of Cement (lb):	422.64
Design Strength (psi):	40+

Mixture Component	**lb/yd^3**	**Specific Gravity**	**Density (pcf)**	**Absolute Vol. (ft^3)**
Potable Water	232.45	1.00	62.40	3.73
Portland Cement (ASTM C150)	422.64	3.15	196.50	2.15
Foam (ASTM 796-97, 869)	73.91	0.05	3.00	24.64
Total	729.00		23.52	31

The values shown in the table vary somewhat from the calculated values from periodic testing of the cellular concrete provided. Figure 4-1 and Figure 4-2 show the measured density of the cellular concrete as recorded during the concrete placement process. The unit weight ended up being slightly higher than the target density of 27 pounds per cubic foot and much higher than the density recorded in the mixture design of 23.52 pounds per cubic foot.

The variation that occurred due to the addition of foam is shown in Figure 4-1 and Figure 4-2. While there was quite significant variation in the density, the biggest variation from 27 pounds per cubic foot especially for the 30° skew test occurred at the very beginning of the pumping stage. This would not affect our test significantly because that is the concrete that is beneath the failure surface. Average density for the two tests were 29.0 pounds per cubic foot and 30.9 pounds per cubic foot for the 0° and 30° tests, respectively.

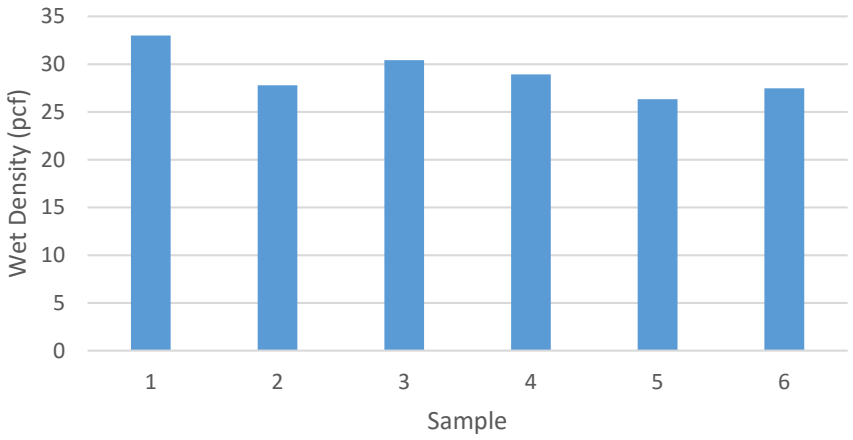

Figure 4-1: Wet density by sample for 0° skew test.

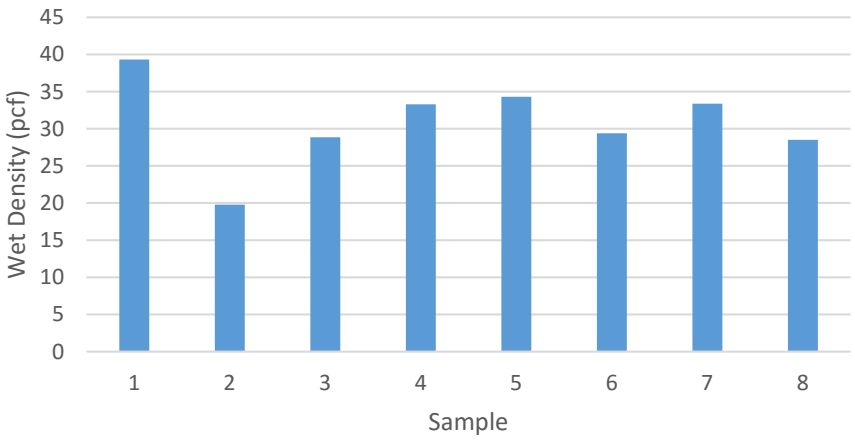

Figure 4-2: Wet density by sample for 30° skew test.

4.2 Laboratory Testing

4.2.1 Unconfined Compressive Strength

Concrete cylinders were cast in 3-in x 6-in Styrofoam molds with the sampling procedure explained in Section 4.1. They were cast in accordance with ASTM C495, with modifications made as outlined in Caltrans Standard Specifications Section 19-10. The cylinders were left to cure in the Styrofoam molds for approximately 72 hours at room temperature in the structures lab before being extracted in accordance with Elastizell recommendations. Figure 4-3 and Figure 4-4 show the extraction process. The Styrofoam box was manually sawn into 4 pieces, after which the base of each piece was scored in a tic-tac-toe pattern and carefully removed. The sides of the mold were then scored and carefully removed. Care was taken to have minimal cuts or disturbance to the cellular concrete cylinders. The extracted cylinders were then labeled and placed in a fog room maintained at a temperature of approximately 73° F (22.8° C).

Figure 4-3 : Extraction of cellular concrete cylinders as per Elastizell recommendations.

Figure 4-4 : Extraction of cellular concrete cylinders from foam molds.

The testing of the cellular concrete cylinders occurred at approximately weekly intervals. The cylinders were also tested on the day of the large-scale laboratory test to compare the UCS of the cylinders with the results of the large-scale testing. At least four cylinders were tested at each testing interval. These cylinders varied in density so that the average of the cylinders was approximately the same as the average of the entire cellular concrete large-scale test.

The cylinders were removed from the fog room 24-72 hours prior to testing to allow them to completely dry. They were capped with gypsum cement, then placed in an unconfined compression test machine as shown in Figure 4-5. Linear variable differential transformers (LVDTs) were placed on each side of a metal plate which was placed on top of the sample. The LVDTs measured the deformation of the cylinder to evaluate if there was uniform deflection of the cylinder. The cylinders were loaded at 0.08 in./min (2.03 mm/min) until obvious failure of the cylinder or until the total deflection of the cylinder was at least 0.5-in (1.27-cm).

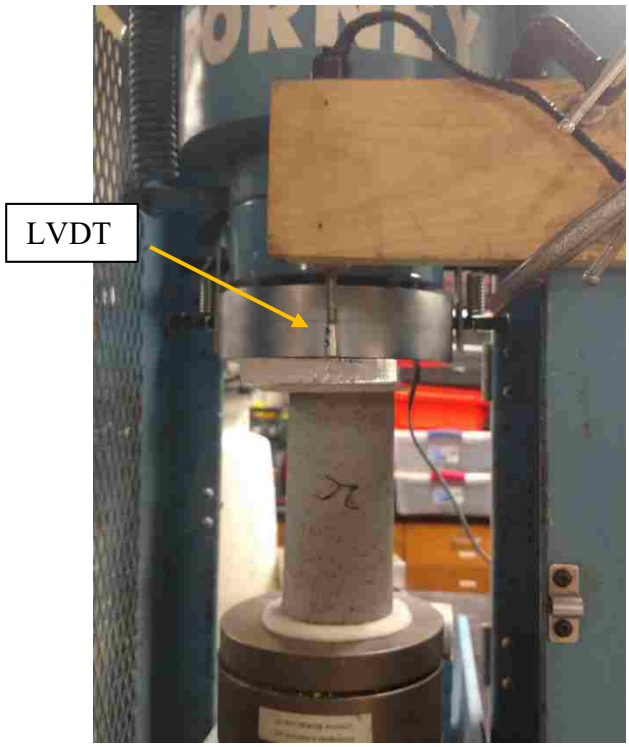

Figure 4-5: Photo of Unconfined Compressive Strength (UCS) testing.

Because of the high residual strength often exhibited by cellular concrete cylinders, peak strength was classified using the 0.2% offset method. This involves taking a line which is parallel with the initial slope of the stress versus strain curve for the cylinder and then offsetting this slope by 0.2% strain. The intersection between this line and the stress versus strain curve for the cylinder is defined as the peak unconfined compressive strength. This method is useful for uniformity among test cylinders that often do not have an easily recognizable peak, as shown in Figure 4-6.

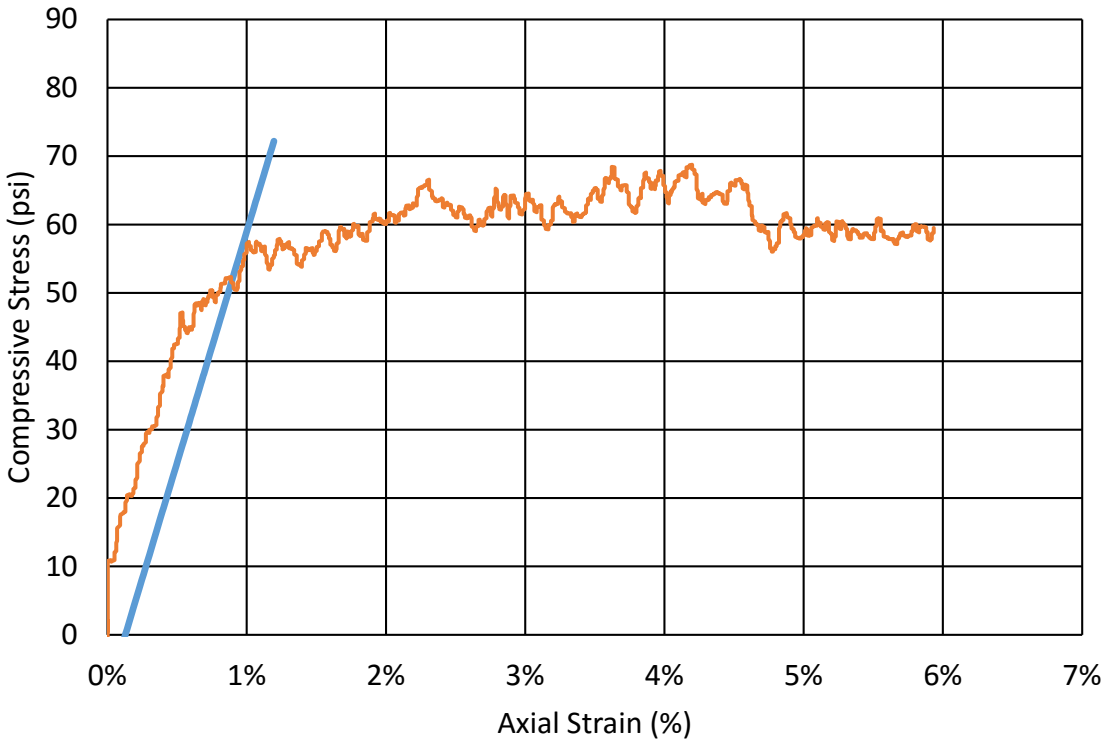

Figure 4-6: Unconfined compressive stress vs. axial strain for a sample cellular concrete cylinder.

A moving average was used to generate the stress versus strain curve and eliminate noise from the unconfined compressive stress machine. A time step interval of 50 was used to create the moving average curve, which corresponds to a strain range of about 0.0017%. While Figure 4-6 is just one example of the many cylinders that were tested, the general shape of the curve is very typical. The compressive stress for nearly all cylinders would increase linearly nearly until the peak compressive stress was reached. Then the compressive stress would remain nearly constant or decrease slightly, but almost never with a significant drop in compressive stress. This is one of the benefits of using cellular concrete. It exhibits a ductile rather than a brittle failure.

4.2.1.1 UCS Test Results

Fifty-four cylinders in total were tested from the 0° and 30° skew cellular concrete tests. A summary of the measured unit weight, cure time, and unconfined compressive strength (UCS) for each cylinder can be found in Table 4-2 and Table 4-3 for the 0° skew and the 30° skew tests, respectively. The average UCS for the 0° skew test on the day that large-scale testing was performed was 70.75 psi. The average UCS for the 30° skew test on the day that large-scale testing was performed was 99 psi. These are the values which are used in subsequent analysis for estimating cohesion values used in the passive force versus deflection curves. It is noted that a longer curing time of the large-scale test would have produced some slight increase in the average UCS. This is discussed in later in this section.

Table 4-2: 0° Skew Cellular Concrete Cylinder Overview

Name of Cylinder	Curing Time (days)	Wet Density (pcf)	Unconfined Compressive Strength (psi)
4A	3	28.9	55
6B	3	26.34	50
6D	3	26.34	52
1A	6	27.8	66
2D	6	27.8	116
6C	6	26.34	51
7B	6	27.5	50
4C	7	28.9	62
4D	7	28.9	62
6A	7	26.34	55
9C	7	27.5	49
9D	7	27.5	51
1B	14	27.8	74
2B	14	30.43	110
3D	14	28.9	64
5D	14	26.34	79
7A	14	27.5	88
1D	22	27.8	129
2A	22	30.43	125
3C	22	28.9	112
5C	22	26.34	95
7D	22	27.5	105
1C	30	27.8	131
2C	30	30.43	113
3A	30	28.9	160
4B	30	28.9	128
5A	30	26.34	127
5B	30	26.34	134
7C	30	27.5	112.5
9A	30	27.5	68

Table 4-3: 30° Skew Cellular Concrete Cylinder Overview

Name of Cylinder	Curing Time (days)	Wet Density (pcf)	Unconfined Compressive Strength (psi)
4A	5	33.29	94
2B	5	28.86	91
4A	5	33.29	91
6A	5	29.39	114
7D	5	34.3	105
2A	7	28.86	73
4D	7	33.29	130
6B	7	29.39	161
7B	7	34.3	93.4
1B	14	19.78	29
2D	14	28.86	86
4B	14	33.29	121
6D	14	29.39	130
7C	14	34.3	120
1C	22	19.78	22
2C	22	28.86	102
7A	22	34.3	134
8A	22	33.4	140
1D	28	19.78	22
4C	28	33.29	169
6C	28	29.39	159
8B	28	33.4	114.2
8C	28	33.4	161
8D	28	33.4	164

Figure 4-7 shows a plot of the unconfined compressive strength (UCS) at 28 days versus wet density, along with the exponential best-fit relationship for 14 data points. The UCS in units of psi is given by the equation

$$UCS = 4.9118\, e^{0.01086\gamma} \qquad \text{Equation 4-1}$$

where γ is the unit weight in lbs/ft^3. This best-fit line as an R^2 value of 0.59.

Figure 4-8 shows a plot of the unconfined compressive strength versus curing time for all test cylinders along with the best-fit linear relationship. UCS in units of psi is given by the equation

$$UCS = 1.9543t + 66.754 \qquad \text{Equation 4-2}$$

where t is curing time in days. This best-fit line has an R^2 value of only 0.24. Both of the R^2 values for these two relationships are low, indicating that only 24 to 59 percent of the variation in compressive strength is explained by the wet density or curing time, respectively. Nevertheless, there is some evidence of a trend in the data for both relationships. As mentioned previously, it is likely that the large-scale test would have had an increase in UCS if it had been left to cure for 28 days instead of 5-6 days.

Cellular concrete is known for being variable in its strength, which is why the testing procedure involves breaking at least four cylinders with every test cycle and using an average. In some cases, more than four cylinders were tested. It can be seen from the figures that there is a significant amount of scatter in the data based on the variability of the material.

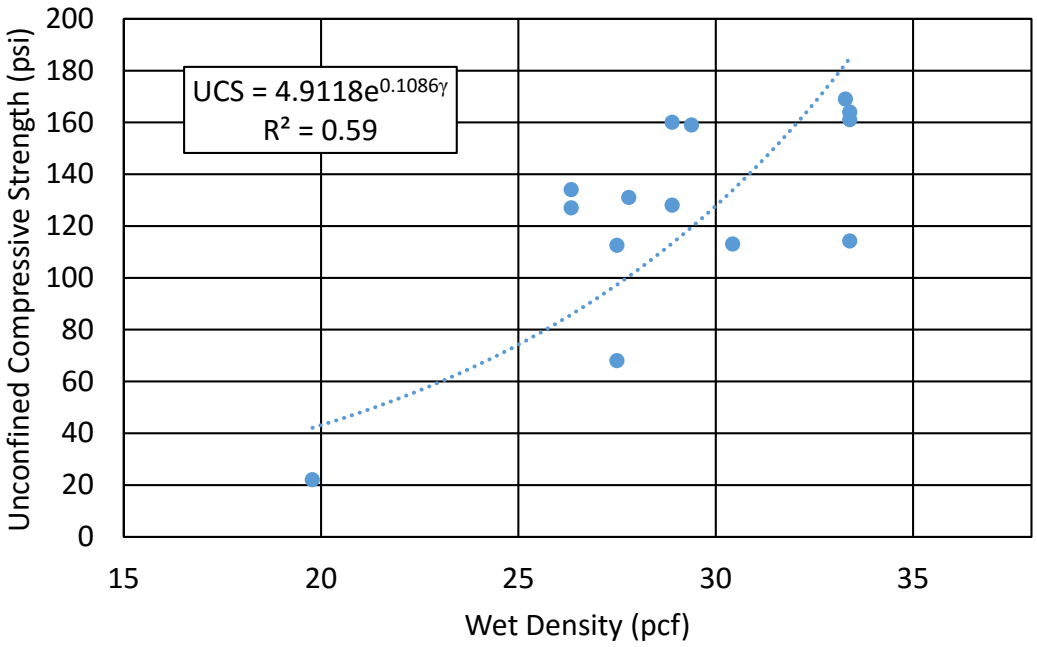

Figure 4-7: Cylinder unconfined compressive strength versus wet density.

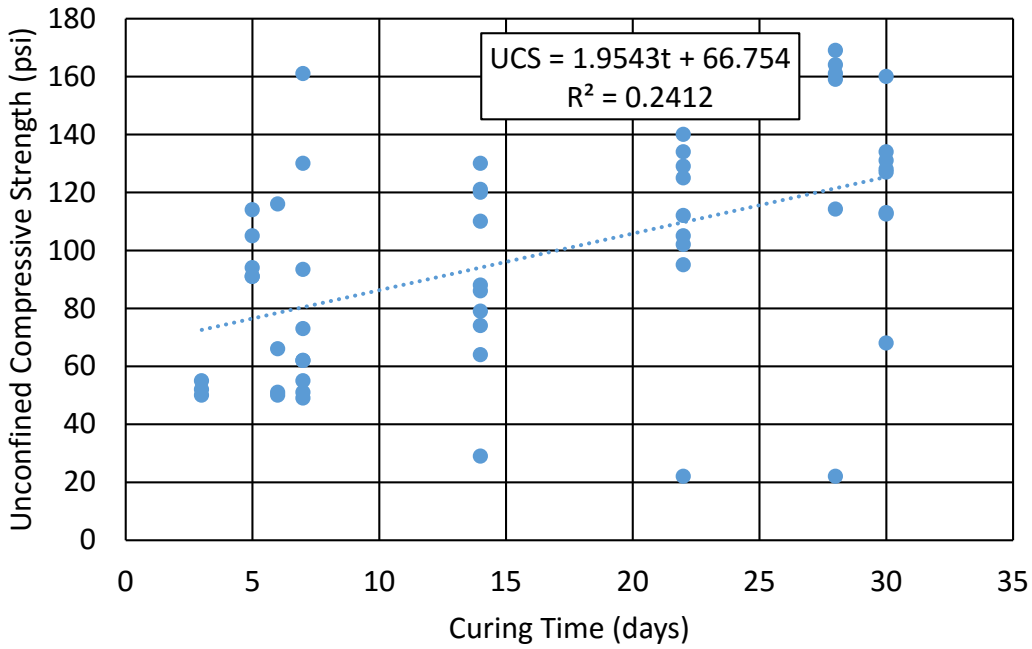

Figure 4-8: Cylinder unconfined compressive strength versus curing time.

Based on the comparison of the R^2 values for UCS and test unit weight for our test, it seems reasonable to use solely the test unit weight for the prediction equation. An equation for predicting unconfined compressive strength (UCS) in kPa units was proposed by Tiwari et al. (2017).

$$UCS = 291.98\,\gamma^2 - 2063.4\,\gamma + 3785 \qquad \text{Equation 4-3}$$

where:

UCS = unconfined compressive strength in kPa

γ = test unit weight in kN/m^3

This method of predicting the unconfined compressive strength was not extremely accurate for our data. The average percent error when using this equation and comparing it to the actual UCS data was 39%. This demonstrates that the strength of cellular concrete is quite variable. However, our data points did fall within ±0.5 standard deviations from the best-fit regression.

Figure 4-9 shows the plot of the best-fit regression equation for predicting unconfined compressive strength as well as lines showing ±0.5 standard deviations. As is evidenced by the figure, all of the points from this study fell within the ±0.5 standard deviation lines. The LCC UCS data from the 28 day tests are shown in blue, while the LCC UCS data from the tests performed on the same day as the large-scale test are shown in red. The data points collected in the cellular concrete test done by Remund (2017) are also included in Figure 4-9. All but one of the data points collected by Remund fall also fall within the bounds of ±0.5 standard deviations from the best-fit regression. This seems to indicate that the method for predicting UCS with test unit weight as proposed by Tiwari et al. is an acceptable method.

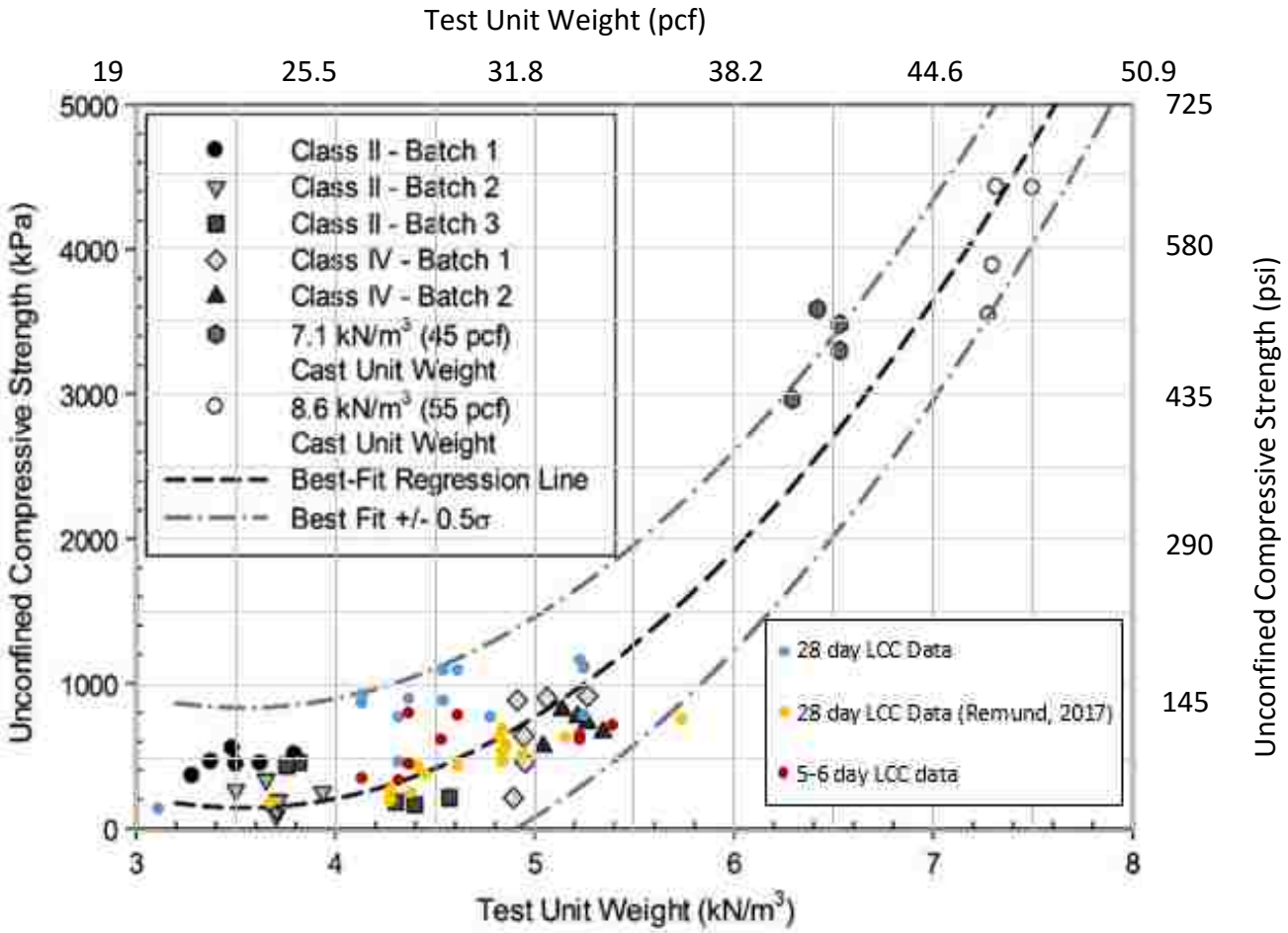

Figure 4-9: LCC data from two Brigham Young University tests compared with results by Tiwari et al. (2017).

4.2.1.3 LVDT Analysis

As mentioned previously, linear variable differential transformers (LVDTs) were placed on each side of a metal plate which was placed on top of the sample. The LVDTs measured the deformation of the cylinder to evaluate if there was uniform deflection of the cylinder. The LVDT deflections were plotted for each cellular concrete cylinder that was crushed. Figure 4-10 shows the LVDT data for a sample cylinder. The orange line and the blue line represent the two LVDTs. The maximum difference between the two lines was evaluated for each cylinder. This maximum difference generally occurred at the end of the cylinder testing, well after the cylinder had either exhibited failure or been deflected greater than 0.5 inches.

Figure 4-10: LVDT deflections for a sample cylinder.

It was found that the maximum difference between the deflections of the two LVDTs was 0.14 in, or 2.38% of total cylinder height. The average difference in deflections was 0.06 in or 1.0% of total cylinder height. Figure 4-11 is a depiction of the maximum deflection between the two LVDTs for each concrete cylinder tested. It is noted that three of the concrete cylinders did not have usable LVDT data. For two of the three this was due to the LVDT reaching its maximum length before completion of the test. For the third there was unusual large scatter likely due to errors in recording. It is assumed that the 0.05 in average is representative of the difference between LVDTs. This difference is not likely to have influenced the data that was gathered on unconfined compressive strength.

Figure 4-11: Maximum difference in LVDT deflection by concrete sample.

4.2.2 Air Content

The air content of the cellular concrete slurry was measured with a pressuremeter in general accordance with ASTM C231. Slight modifications to the process were made to accommodate the extremely porous cellular concrete. Both petcocks were closed to keep the water from sinking into the material. Additionally, the pressuremeter was tapped by hand after the placement of each of the two lifts instead of rodding or vibration. It is noted that the accuracy of this method for measuring air content may be somewhat inaccurate due to the extremely lightweight nature of the material, however the results obtained seem to conform to the expected air content values based on the amount of foam added to the cement slurry. A summary of air contents measured throughout the cellular concrete placement process is shown in Table 4-4 and Table 4-5 for the 0° and 30° skew tests, respectively. The measured values were between 60-65% air. However, according to Table 2-2 the expected air content would be around 75%.

Table 4-4: 0° Skew Air Content

Test	Air Content (%)
1	65
2	65

Table 4-5: 30° Skew Air Content

Test	Air Content (%)
1	61
2	63
3	60

4.2.3 Flowability

Flow diameter tests were performed in general accordance with ASTM D6103 (Standard Test Method for Flow Consistency of Controlled Low Strength Material). The flow diameters for each batch/ interval are shown in Table 4-6. The average flow diameter for the 0° skew test was 8.8 in. (223.3 mm), and the average flow diameter for the 30° skew test was 7.9 in. (201.6 mm.). Flow diameters of 8 indicate good flowability for a controlled low strength material. Both tests averaged around 8 in. for flow diameter, indicating that they have good flowability for placement of the material with no need for vibration.

Table 4-6: Flowability of Cellular Concrete

Cellular Concrete Test	Batch/ Interval	Flow Diameter (in.)	Flow Diameter (mm.)
0° Skew	1	9.25	234.95
	2	8.375	212.725
	3	8.375	212.725
	4	9.375	238.125
	5	8.375	212.725
	6	9	228.6
30° Skew	1	10	254
	2	6.75	171.45
	3	7.5	190.5
	4	7	177.8
	5	8.25	209.55
	6	7.75	196.85
	7	8.25	209.55
	8	8	203.2

4.2.4 Curing Rate

Curing rate of the cellular concrete was measured with thermocouples as outlined in Section 3.3.5. One thermocouple lead wire was placed in a test cylinder in a Styrofoam block of the same type used to make the samples for the Unconfined Compressive Strength test. This block was placed in a plastic cooler next to the test box to ensure that it was not disturbed. The other three thermocouple lead wires were placed approximately 6 in. from the back wall of the test box at depths of 6 in., 18 in., and 27 in. from the top of the fill. The cellular concrete in the 0° skew test reached a peak temperature between 14 and 19 hours after placement as shown in Figure 4-12. The cellular concrete in the 30° skew test reached a peak temperature at 18 hours as shown in Figure 4-13. The highest temperatures were developed in the center of the fill as expected. The temperature approaches the ambient value at all depths after about 140 hours.

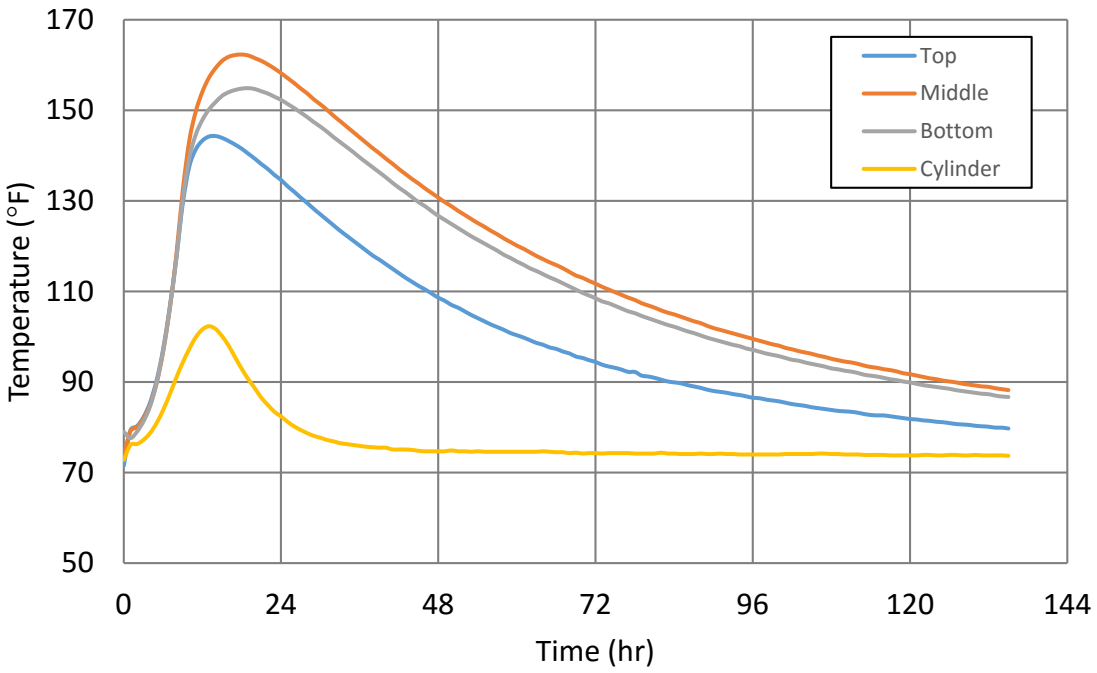

Figure 4-12: Temperature vs. time for 0° skew test.

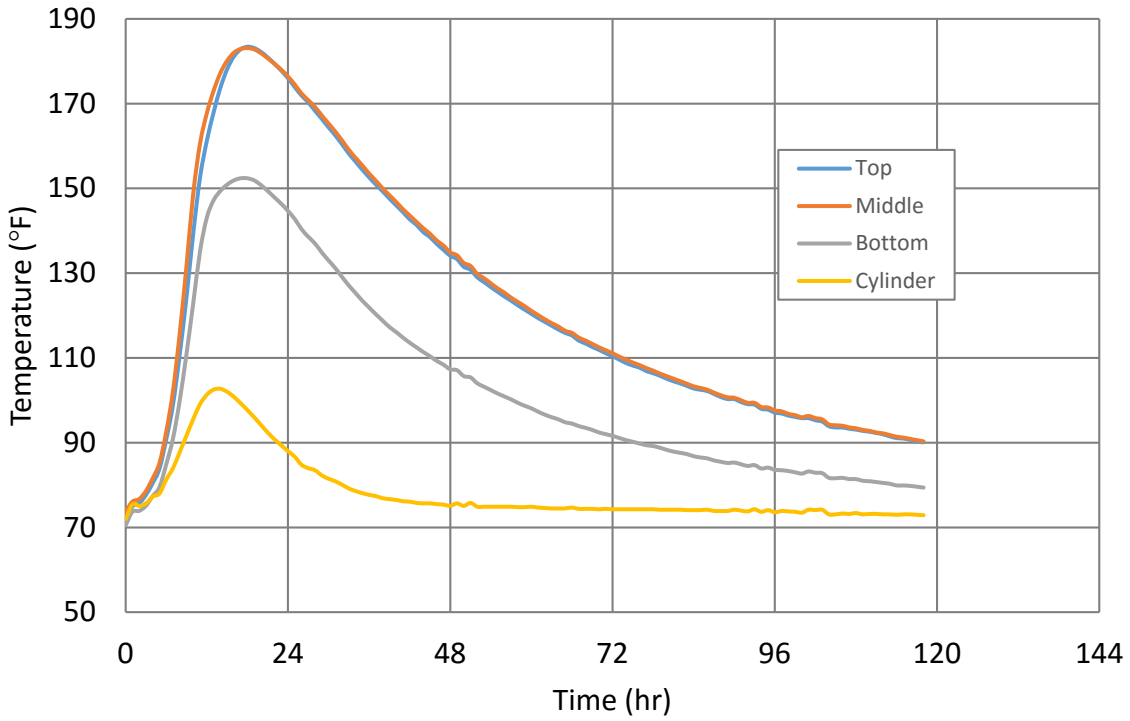

Figure 4-13: Temperature vs. time for 30° skew test.

The temperature of the cellular concrete at three depths is shown for 0 hours, 10 hours, 18 hours, 25 hours, 50 hours, and 100 hours for the 0° skew test and the 30° skew test in Figure 4-14 and Figure 4-15, respectively. Both tests have similar patterns with a high early temperature increase followed by a decrease after 25 hours. The most notable difference between the two skew tests is that for the 0° skew test the temperature gage at 6 inches below the surface of the fill reached a higher temperature at 10 hours than at 25 hours. Normal temperature variation in curing of concrete likely accounts for this difference.

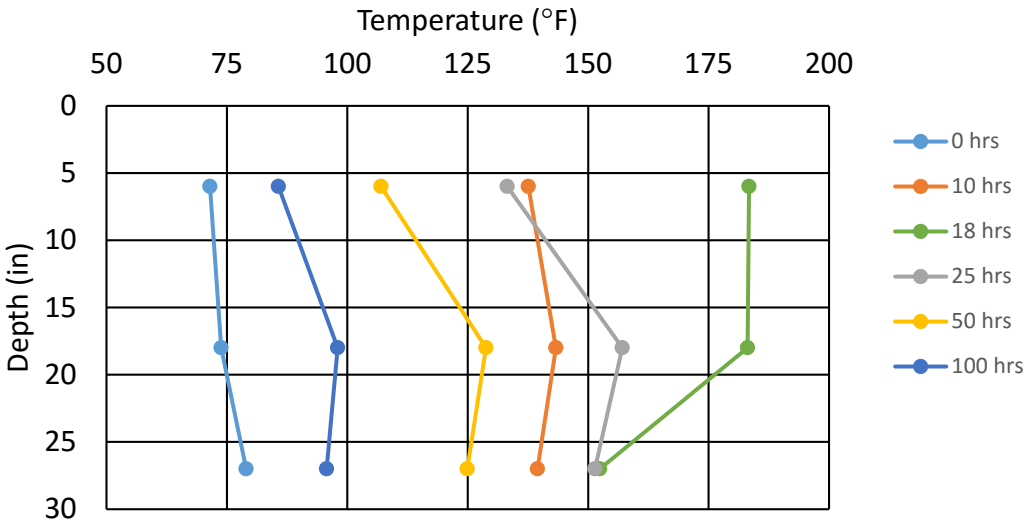

Figure 4-14: Temperature vs. depth for 0° skew test.

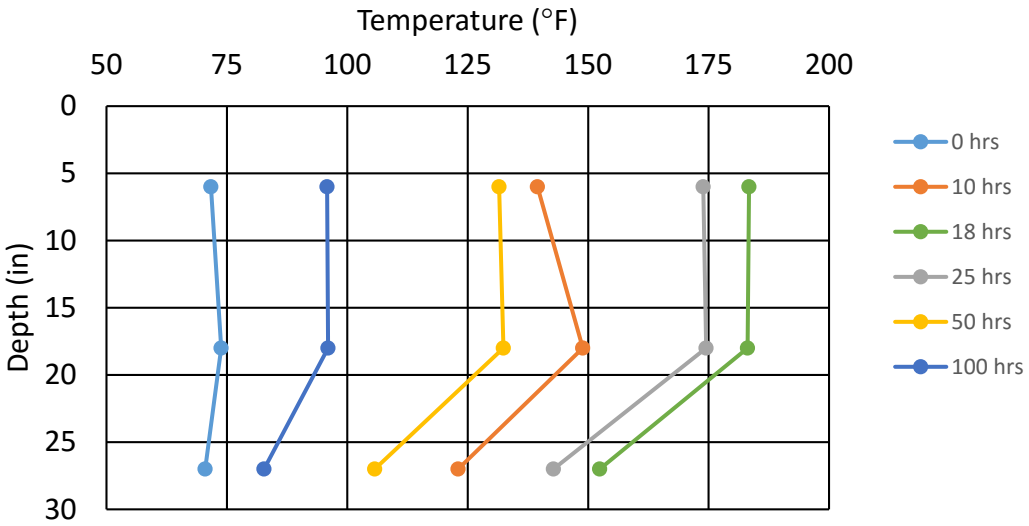

Figure 4-15: Temperature vs. depth for 30° skew test.

5 PASSIVE FORCE TEST RESULTS

5.1 Force-Deflection Curves

Longitudinal force induced by the actuator and displacement of the backwall were obtained during the large scale test for both the 0° skew and the 30° skew test. The load from the actuator as the backfill was compressed was measured with a calibrated pressure transducer and recorded with a computer data acquisition system. The longitudinal displacement of the backwall was measured with the four string potentiometers which were attached to the backwall as described in Section 3.3.3. An average of the four string potentiometer displacements was used to define the displacement of the backwall. Although there was some small rotation of the backwall, it is assumed that the average of the string potentiometer provides the best measure of displacement. The data measured during the large scale cellular concrete tests was analyzed to create passive force versus deflection curves for each test. The passive force was determined with the following equation proposed by Burke (1994) to resolve the longitudinal force normal to the wall face:

$$P_P = P_L \cos\Theta \qquad \text{Equation 5-1}$$

where:

P_P = Passive Force

P_L = Longitudinal Force (as measured with actuator)

Θ = Skew Angle

Figure 5-1 shows the passive force vs. deflection for both the 0° skew and the 30° skew cellular concrete tests. The 30° skew test showed a decrease in passive resistance as compared to the 0° skew. This conforms with results of skewed abutment testing with granular backfills that has been reported by Rollins and Jessee (2013). It is also consistent with predicted skew effects for granular fills based on finite element analyses conducted by Shamsabadi, Rollins and Kapuskar (2007).

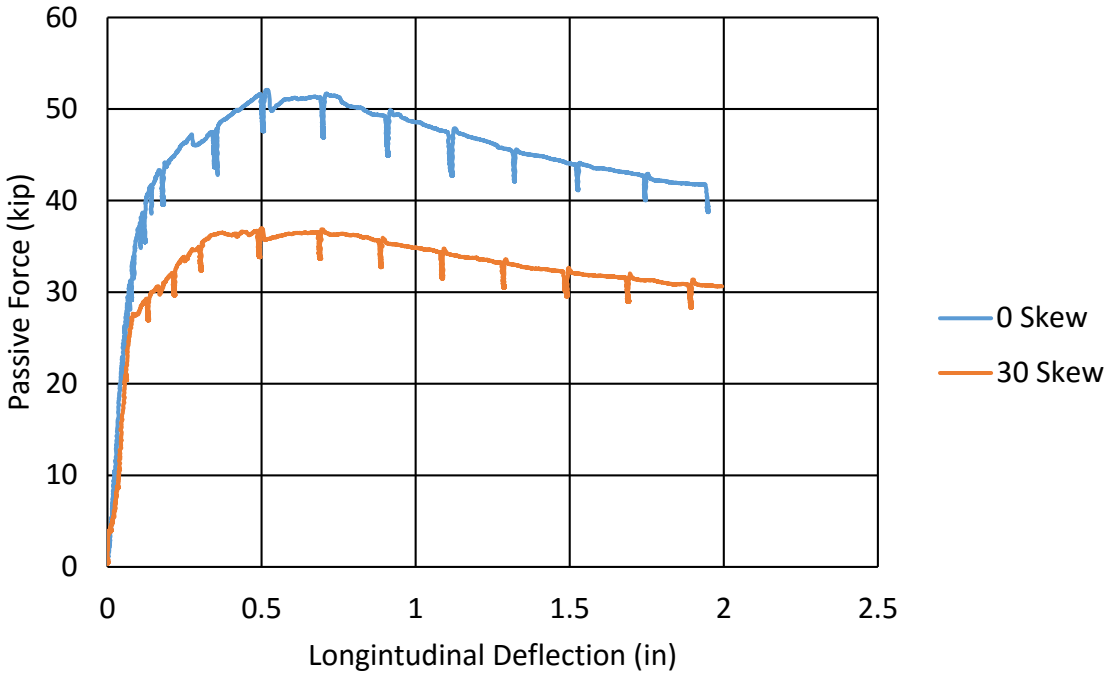

Figure 5-1: Passive force-deflection curves for cellular concrete tests.

The results of the two cellular concrete tests do not agree with the skew test results on cellular concrete performed at a larger scale reported by Remund (2017). It should be noted that the predicted reduction in passive force occurred even though the average 28-day unconfined compressive strength of the cellular concrete used in the 30° skew test was 10% higher than the 28-day unconfined compressive strength of the cellular concrete used in the 0° skew test. A 13%

higher unconfined compression strength was proposed by Remund to explain why he observed a higher peak passive force in the 30° skew test that he performed relative to a companion 0° skew test. However, it does not appear that the higher unconfined compressive strength of the 30° skew cellular concrete in this study increased the peak passive resistance of the large scale test enough to make it higher that the peak passive resistance observed in the 0° skew test.

The cellular concrete for the 0° skew test reached a maximum passive force of 52 kips at a displacement of 0.51 inches of deflection or about 0.02 times the height of the backwall. The cellular concrete for the 30° skew test reached a maximum passive force of 37 kips after approximately the same displacement (0.50 in). The peak resistance for each test as well as the measured displacement at the peak is recorded below in Table 5-1.

Table 5-1: Force-Deflection Results for 0° Skew and 30° Skew Tests

Test	Measured Peak Load (kips)	Measured Displacement to Peak Load (in)	Deflection at Peak Load (%H)
0° Skew	52.1	0.51	2.13
30° Skew	37.0	0.50	2.08

Table 5-2, gives a summary of initial stiffness in kips/in per foot of wall width. This corresponds to the initial slope of the force-deflection curve which is relatively linear. As shown in the table below, the measured stiffness for the two tests is similar (within 12%) but not identical. However, for later calculations with PYCAP it is assumed that a similar measured stiffness can be used for the two tests.

Table 5-2: Stiffness and Initial Resistance

Test	Measured Initial Load (kips)	Measured Displacement to Initial Load (in)	Measured Stiffness (kips/in/ft)
0° Skew	38.0	0.121	76
30° Skew	26.0	0.074	85

Figure 5-2 provides a comparison between the passive force-deflection curve for the 0° skew cellular concrete and those for compacted sand and flowable fill backfills. All of these tests were performed using a similar box and testing procedure. The sand backfill was clean poorly-graded sand classifying as SP according to the United Soil Classification System and A-1-b according to the AASHTO system. The sand was compacted to 110.8 lbs/ft^3 or about 98% of the modified Proctor maximum density (113.3 lbs/ft^3) at an optimum moisture content of approximately 8% (Jessee 2012). A correlation developed by (Lee and Singh 1971) suggests that the sand was at a relative density of approximately 90%. The flowable fill (CLSM) had a unit weight of 124 lbs/ft^3 and an unconfined compressive strength of 85 psi at time of testing (Wagstaff 2016).

The initial stiffness, peak passive force, and deflection at peak load are summarized in Table 5-3. Data was obtained from tests by Jesse (2012) and Wagstaff (2016).

Table 5-3: Summary of Passive Force and Stiffness for Various Materials Obtained from Large-Scale Laboratory Testing

Material	Initial Stiffness (kips/in/ft)	Peak Load (kips)	Deflection at Peak Load (in)	Deflection at Peak Load (%H)
Cellular Concrete	76	52	0.51	2.1
Clean Sand	32.5	45	0.80	3.3
Flowable Fill	325	61	0.50	2.0

The initial stiffness of the cellular concrete is just over twice that of compacted sand and approximately one tenth times that of flowable fill. However, the deflection at peak load for cellular concrete is relatively similar to the other backfill materials. As shown in Figure 5-2, the peak passive resistance is obtained for all three tests between 0.5 and 0.8 inches, or between about 0.02 and 0.035 times the height of the backwall. The curve for the cellular concrete is very similar to the curve observed by Jessee (2012) using compacted sand. However, the test with flowable fill produced a curve with a higher peak passive resistance but also a much more significant drop in strength after the peak passive resistance was reached. This demonstrates that cellular concrete exhibits a ductile failure as opposed to a brittle failure exhibited by traditional higher-strength concretes. This characteristic can be extremely beneficial for a material which is subject to seismic loadings.

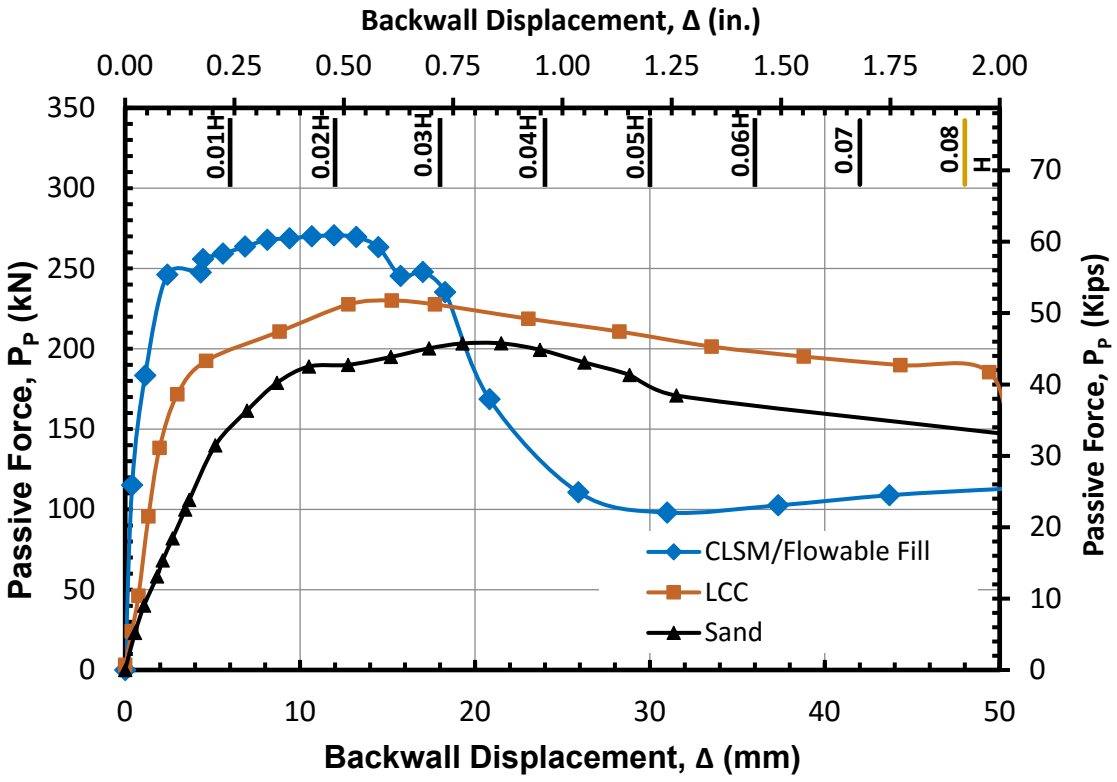

Figure 5-2: Passive force versus displacement for three materials.

5.2 Surface Heave

Figure 5-3 and Figure 5-4 depict the surface heave contours for the 0° skew test and 30° skew test, respectively. The surface failure plane is also shown. As the figures demonstrate, the heave gradually increases from the backwall face and is the highest where the failure surface daylights. This is the location where the failure wedge impinges against the zone behind the wedge which is relatively stationary. This occurs at a distance of 7.25 ft. from the backwall of the 0° skew test and 5.5 ft. from the center of the backwall for the 30° skew test. This corresponds to a horizontal distance of about 2.75 to 3.75 times the height of the backwall.

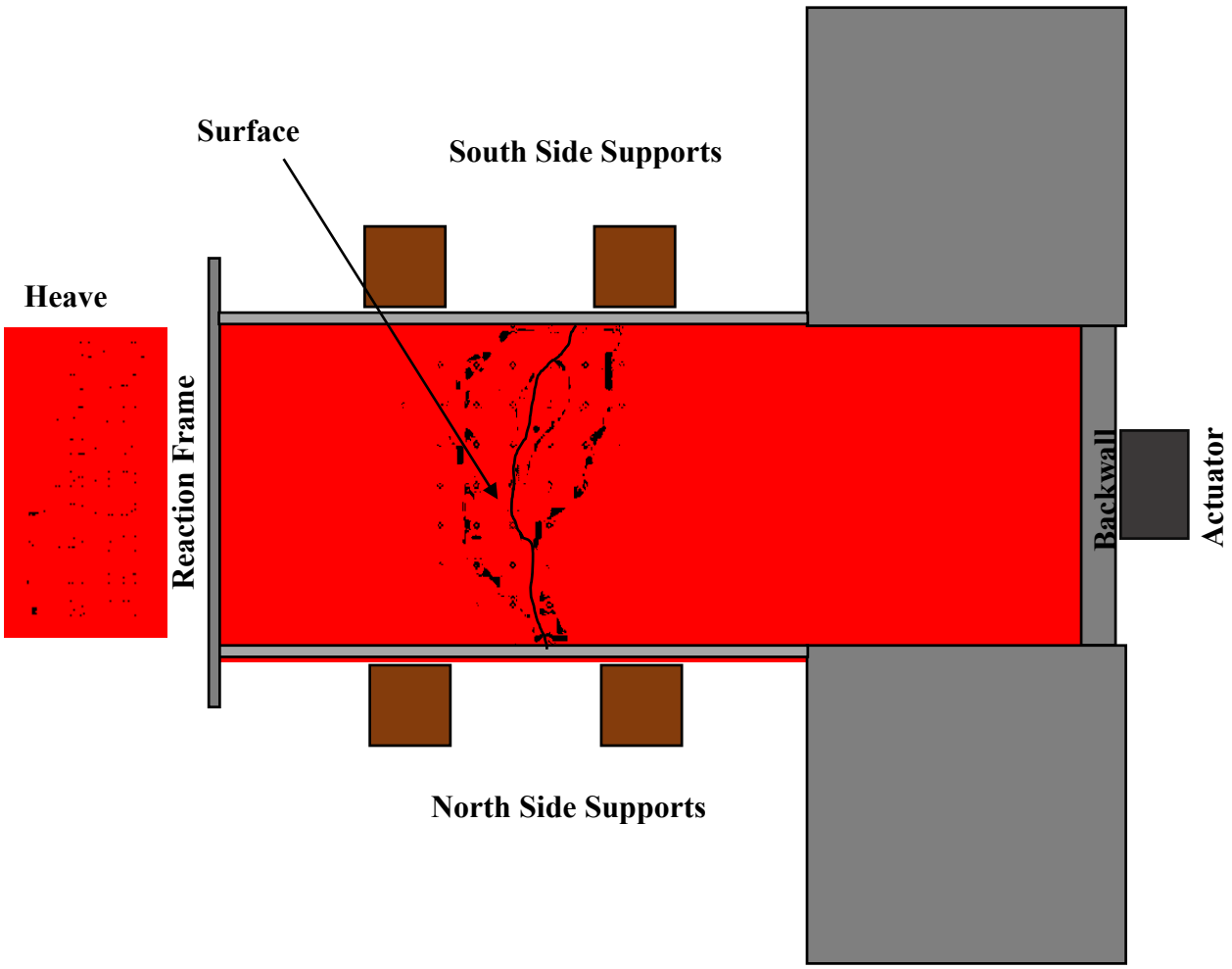

Figure 5-3: Surface heave contours for the 0° skew test.

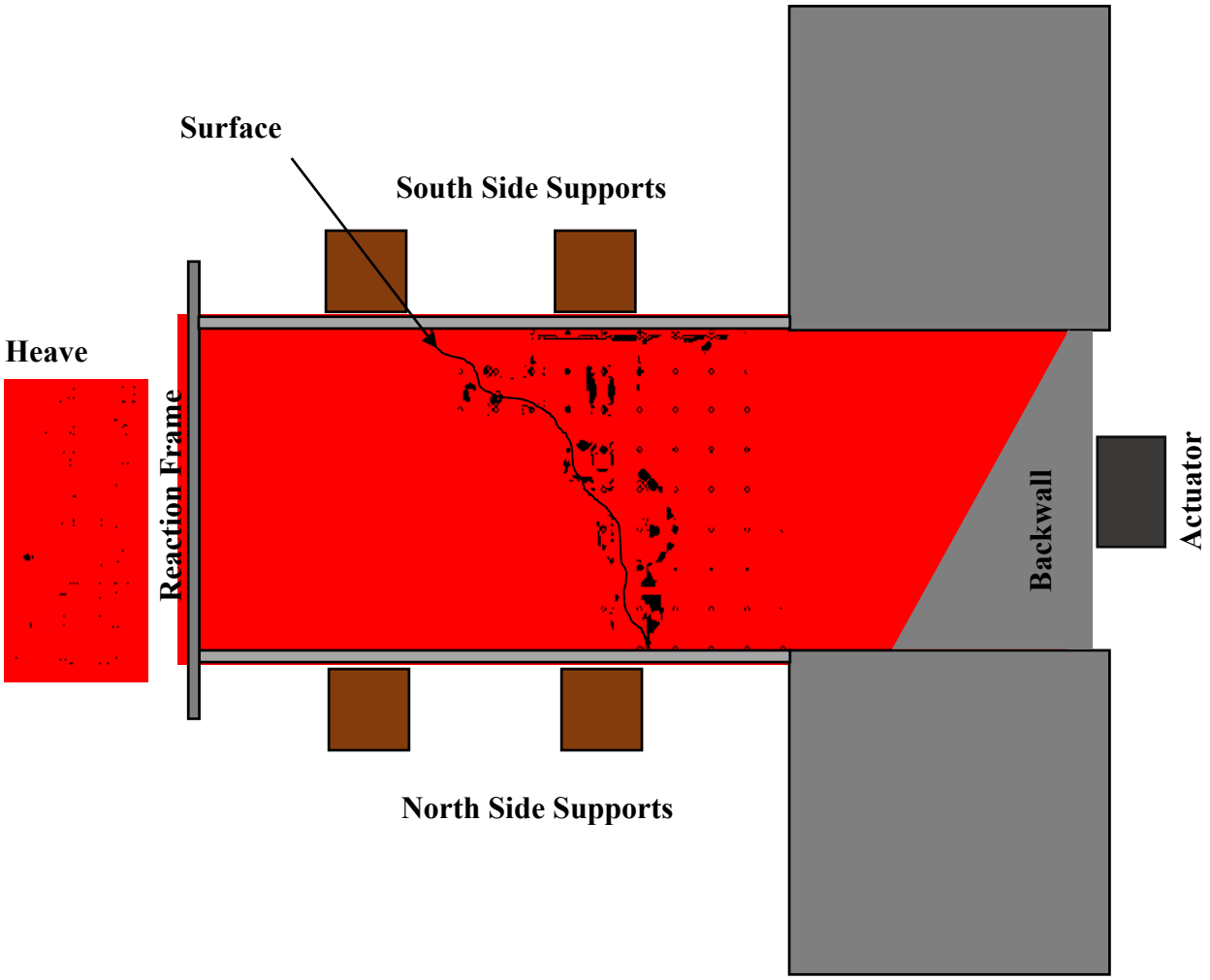

Figure 5-4: Surface heave contours for the 30° skew test.

The failure surface for the 0° skew test was approximately parallel to the backwall and reaction frame. However, the failure surface for the 30° skew test is not parallel to the backwall nor the reaction frame. It exhibits a failure surface of 30° in the direction opposite of the 30° skew. This trend has been observed in a previous test performed by Marsh (2013), although not to the same degree of skew. Figure 5-5 and Figure 5-6 show photos of the 0° skew surface failure and the 30° skew surface failure, respectively. Surface cracking can be observed for both of the tests, along with the surface failure plane. The painted grid provides a way to determine the locations of the surface failure planes.

Figure 5-5: Failure surface of the 0° skew test.

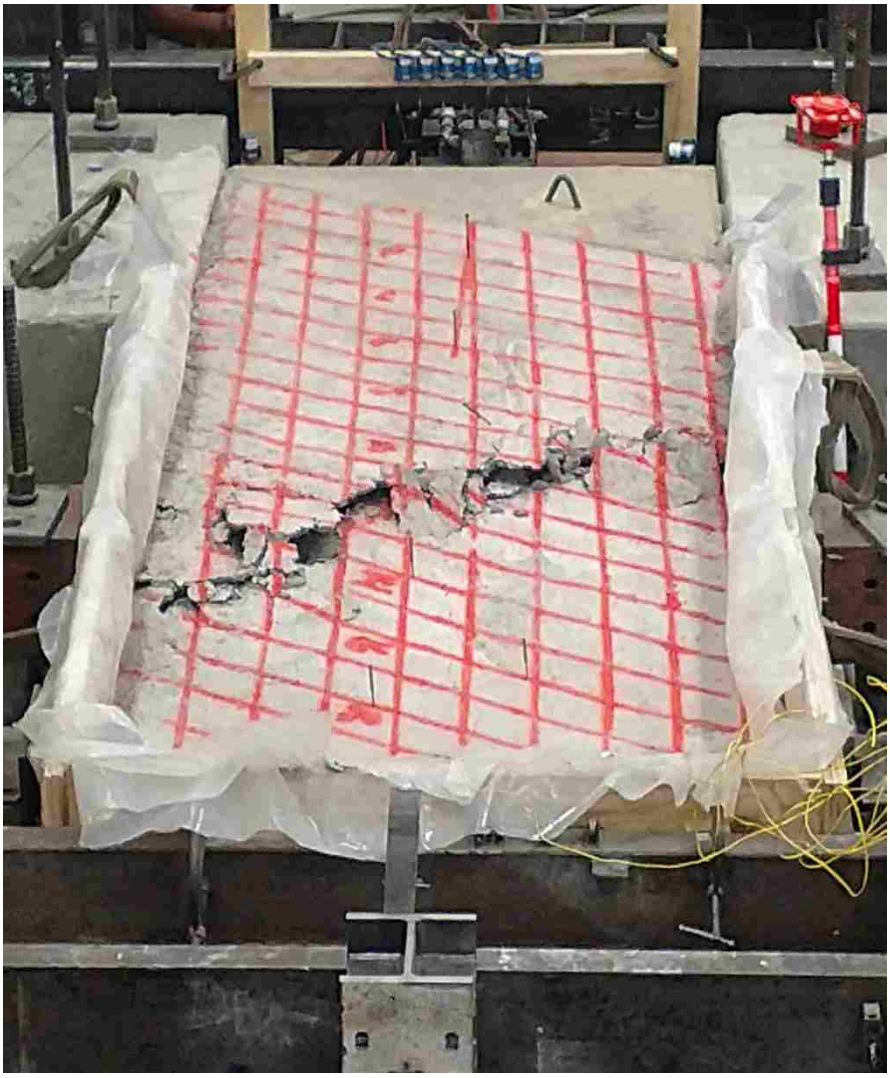

Figure 5-6: Failure surface of the 30° skew test.

5.3 Surface Displacement and Strain

Figure 5-7 shows the horizontal displacement of the backfill at six different backwall displacements for the 0° skew test. If there was no compression in the backfill material, each of the lines would be purely horizontal. From the backwall to one foot behind the wall, the LCC fill compresses an average of 2%. However, between one and six feet there is very little compression, likely indicating that the fill is moving as a rigid mass. The greatest backfill movement clearly occurs in the section of the cellular concrete before the failure surface as shown in Figure 5-7. There is a significant decrease in horizontal displacement between 6 and 8 feet from the backwall. This corresponds to the observed failure surface at 7.25 feet from the backwall. Usable data was not obtained from the 30° skew test for surface displacement and strain, however it is likely that a similar pattern was exhibited with a majority of the displacement and strain occurring before the surface crack. A complication with the 30° skew test could be the angle of surface failure. This could affect the horizontal displacements based on the location of the string potentiometers.

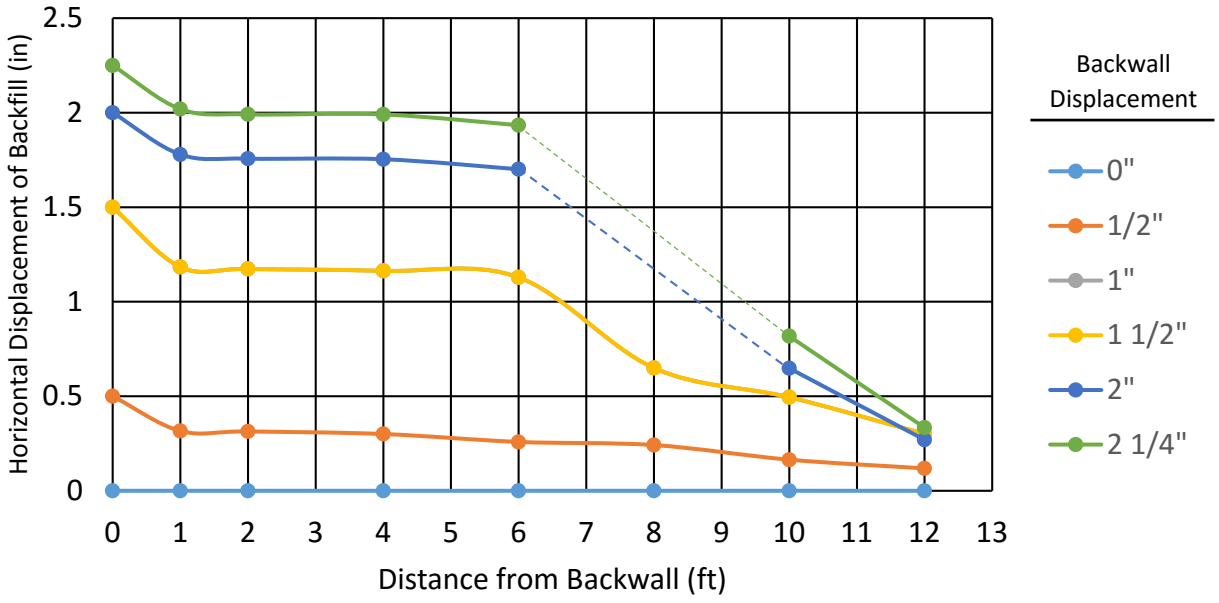

Figure 5-7: Plot of horizontal backfill displacement versus distance from the backwall for the 0° skew test at selected backwall displacements from string potentiometers.

5.4 Failure Surface Geometry

As was mentioned previously, the test box was not disassembled for the 0° skew test. This meant that the failure surface within the fill mass could not be observed, only extrapolated. If the LCC backfill exhibited a Rankine type failure plane, the failure surface would be at an angle of 15°, as shown in Figure 5-8. If the LCC backfill exhibited a log-spiral type failure plane, the failure surface would likely be somewhere in the range of 15° to 30°. Figure 5-9 shows a possible log-spiral type failure plane at an angle of 28°.

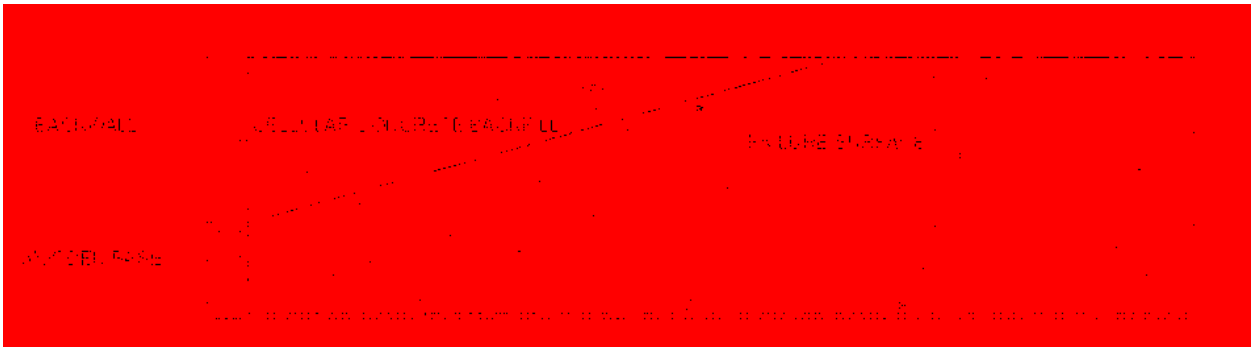

Figure 5-8: Rankine type failure plane for 0° skew test.

Figure 5-9: Log-spiral type failure plane for 0° skew test.

The 30° skew test failure surfaces on both the north side and the south side were approximately 28° as shown in Figure 5-10. The south failure surface is slightly more difficult to assign an angle to, as the curve could vary from approximately 20° to 45°. However, it appears that 28° fits the surface well and matches with the angle observed on the other side of the test. Figure 5-11 is a photo of the north side of the skew, which exhibited a linear Rankine type failure plane. Figure 5-12 and Figure 5-13 are photos of the south side of the test. It exhibits a similar failure surface angle of approximately 28°. However, the south side of the test exhibited a log-spiral type failure plane.

Figure 5-10: Failure surfaces for the LCC 30° skew test.

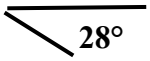

Figure 5-11 : Photo of the failure surface of the 30° skew cellular concrete test (north side).

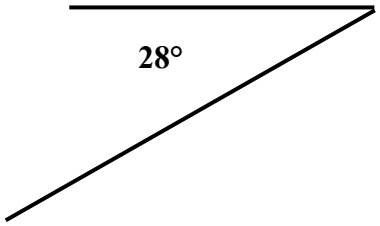

Figure 5-12: Photo of the failure surface of the 30° skew test (south side).

Figure 5-13: Photo of log-spiral behavior of 30° skew test failure plane.

5.5 Backwall Rotation

As mentioned in Section 3.3.3, string potentiometers were used to monitor any rotation of the backwall that occurred during actuator loading. It was found that for the 0° skew test the maximum rotation about the horizontal backwall axis was approximately 0.7°. The bottom of the backwall rotated this slight amount more into the cellular concrete backfill than the top of the backwall. The maximum rotation about the vertical backwall axis was approximately 0.1°. The 30° skew test exhibited a maximum rotation about the horizontal backwall axis of approximately 1°, again with the bottom of the backwall rotating in towards the cellular concrete. The maximum rotation about the vertical backwall axis was approximately 0.1°, with the north side (the obtuse angle of cellular concrete), rotating into the cellular concrete towards the south side. Plots of the

rotation of backwall versus backwall displacement are shown in Figure 5-14 and Figure 5-15 for the 0° skew test, and Figure 5-16 and Figure 5-17 for the 30° skew test. Because the degree of rotation is so small in all cases, it is unlikely that rotation of the backwall had a significant effect on the results of the large-scale test.

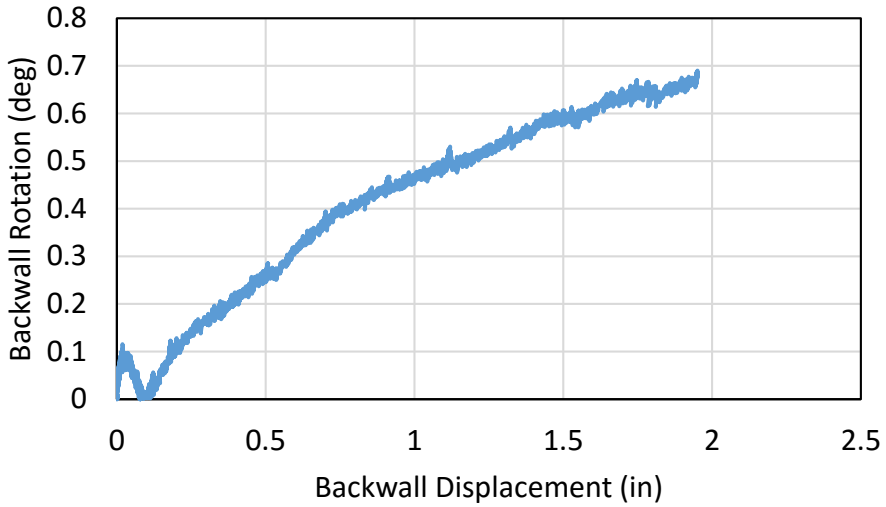

Figure 5-14: Backwall rotation about a horizontal axis versus backwall displacement for the 0° skew test.

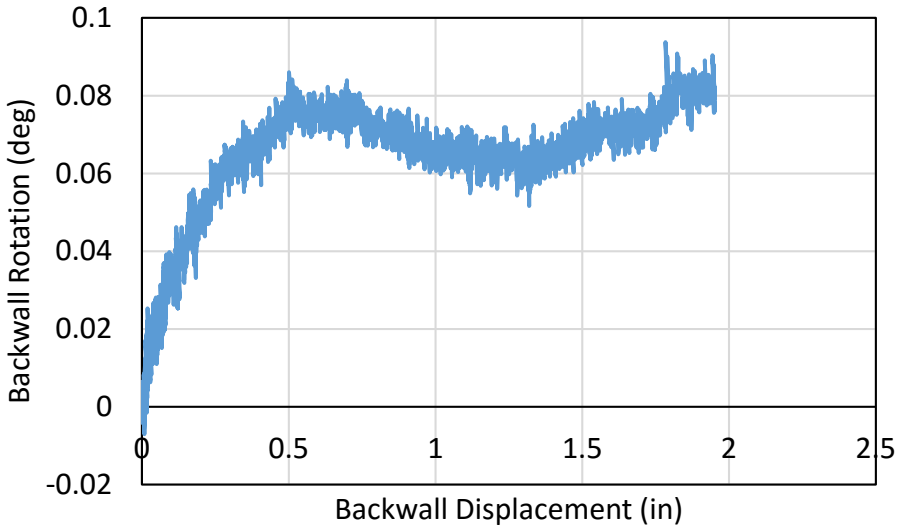

Figure 5-15: Backwall rotation about a vertical axis versus backwall displacement for the 0° skew test.

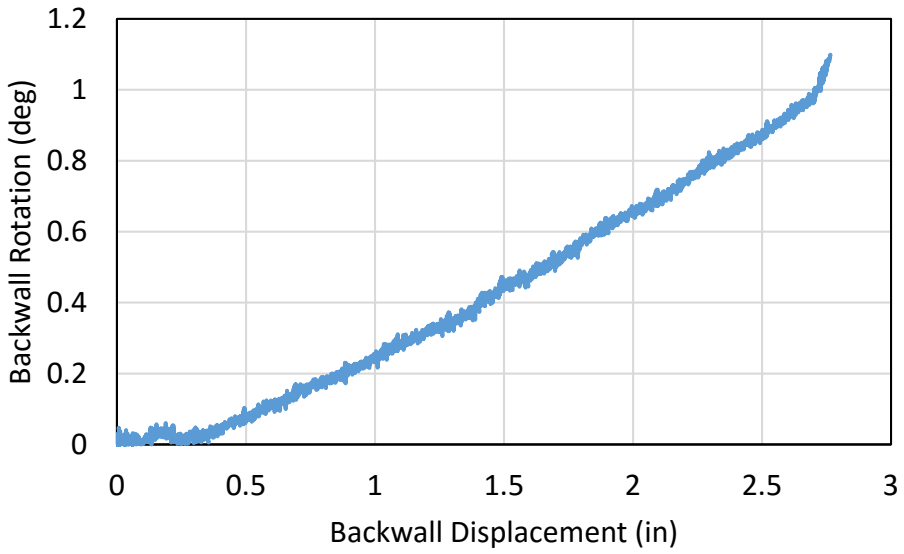

Figure 5-16: Backwall rotation about a horizontal axis versus backwall displacement for the 30° skew test.

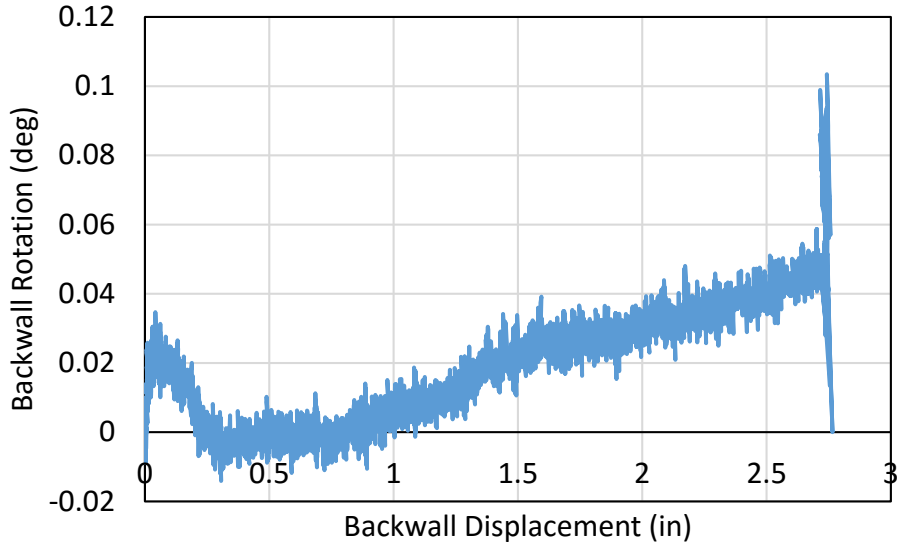

Figure 5-17: Backwall rotation about a vertical axis versus backwall displacement for the 30° skew test.

6 ANALYSIS OF RESULTS

6.1 Skew Reduction Factor

A skew reduction factor (R_{skew}) for the analysis of the 30° skew LCC was calculated based on the correlation for granular backfill by Shamsabadi and Rollins (2014).

$$R_{skew} = \frac{P_{p-skew}}{P_{p-no\ skew}} = e^{\left(\frac{-\theta}{45°}\right)} \qquad \text{Equation 6-1}$$

where:

Θ = degree of skew

P_p = peak passive force

However, there is a discrepancy in R_{skew} values obtained with this equation for the LCC data.

$$R_{skew} = e^{\left(\frac{-\theta}{45°}\right)} = e^{\left(\frac{-30°}{45°}\right)} = 0.5$$

$$R_{skew} = \frac{P_{p-skew}}{P_{p-no\ skew}} = \frac{37\ kip}{52\ kip} = 0.7$$

If the ratio of peak passive forces is used, a value of 0.7 is obtained for R_{skew}. In a study performed on cement-treated gravel by Schwicht (2018), the R_{skew} value was calculated to be 0.76. There is very limited data to determine if 0.7 is an accurate value for R_{skew} of LCC. However, 0.7 is the value that will be used in the subsequent analysis of this thesis. Further analysis should be performed to determine if an R_{skew} value of 0.7 is more accurate than 0.5.

6.2 Rankine Equation Analysis [φ = 0 and c = *f*(UCS/2)]

To evaluate methods of predicting peak passive resistance, a variation of the Rankine method equation was used as follows:

$$P_p = (0.5\gamma H^2 B + 2c'HB) * R_{skew} \quad \text{Equation 6-2}$$

where:

P_p = predicted peak passive resistance

γ = wet density of cellular concrete backfill

H = height of backwall

B = width of backwall

c'= cohesion of concrete, estimated by 0.7 times 50% of the unconfined compressive strength of cylinders broken on the same day as the large scale test.

R_{skew} = skew reduction factor, assumed to be 1 for the 0° skew test and 0.7 for the 30° skew test

When using this equation to predict peak passive resistance, the first term involving backfill weight contributes very little to the peak passive resistance. For both the 0° skew test and for the 30° skew test it accounts for less than 1% of the total passive resistance. Because of this, it is extremely valuable to have an accurate estimation of the cohesion value for the cellular concrete backfill.

Based on experience with shear strength of soil-cement mixtures, Filz et al. (2015) recommended that shear strength be estimated as 0.7 times of 50% of the UCS. The 0.7 factor is used to account for a reduction in strength of the mass relative to that obtained from small test cylinders. This method did not provide extremely accurate results. The peak passive resistance was over predicted for the 0° skew test and the 30° skew test by 14% and 56%, respectively. This

method was also used to predict the peak passive force for the 0° skew test performed by Remund (2017). The 30° skew airport test was not analyzed, because the R_{skew} factor of 0.7 which is applied to the structures lab test is not applicable to that test.

Table 6-1: P_p Prediction

Test	P_p Predicted (kip)	P_p Observed (kip)	Percent Error (%)
2018 Structures Lab 0° skew	59.1	52.1	14%
2018 Structures Lab 30° skew	57.9	37.0	56%
2017 Airport 0° skew	335.2	383.7	13%

6.3 PYCAP Analysis

To more efficiently compute the passive force versus deflection curve with the log-spiral method, the program PYCAP was used. Basic parameters used in PYCAP are summarized in Table 6-2. Cap width, height, embedment depth, and surcharge were all known values based on the geometry of the test layout. The initial soil modulus, E_i, controls the initial slope of the computed passive force-deflection curve. Based on trial and error, E_i was found to be about 2100 kip/ft^2 for all of the iterations done using PYCAP. Poisson's ratio, ν, was assumed to be 0.15, but had relatively little effect on the results. Backfill unit weight was the average wet density of the samples taken during the large-scale pour for each respective test. Adhesion factor was 0. The value of $\Delta max/H$ was the observed value of 0.02. Input values for cohesion, soil friction angle, and wall friction vary between analysis methods and are discussed in each subsection of 6.2. It is noted that

because PYCAP uses a hyperbolic curve to model the passive force-deflection curve, it cannot account for the post-peak softening observed in the large-scale test.

Table 6-2: PYCAP Input Parameters

Input Parameters	0° Skew	30° Skew
cap width, b (ft)	4.13	4.13
cap height, H (ft)	2.00	2.00
embedment depth, z (ft)	0.00	0.00
surcharge, q_s (psf)	0.0	0.0
cohesion, c (psf)	varies	varies
soil friction angle, φ (deg.)	varies	varies
wall friction, δ (deg.)	varies	varies
initial soil modulus, E_i (kip/ft^2)	2100	2100
poisson's ratio, ν	0.15	0.15
LCC unit weight, γ_m (pcf)	29.0	30.9
adhesion factor, a	0	0
Δmax/H	0.02	0.02

6.3.1 PYCAP Analysis with Pure Cohesion

For the first PYCAP analysis, the soil friction angle and wall friction were both assumed to be 0. This is the method used by Remund (2017) and Wagstaff (2016). The value for cohesion was assumed to be 0.7 times 50% of the unconfined compressive strength as proposed by Filz et al. (2015). Table 6-3 gives the PYCAP strength input values based on UCS tests at the time of testing. Figure 6-1 and Figure 6-2 provide graphs of the passive force-deflection curves computed by PYCAP along with the measured curves for the 0° and 30° skew tests, respectively. The 30° skew test includes the 0.7 skew reduction factor. Figure 6-3 compares the PYCAP predicted curve with the measured curve observed by Remund (2017). This method over predicts the peak passive force

for the 0° skew test and the 30° skew test performed for this study. It slightly under predicts the peak passive force for the 0° skew test for Remund (2017).

Table 6-3: Pure Cohesion PYCAP Inputs

Input Parameters	0° Skew	30° Skew
cohesion, c (psf)	3566	4990
soil friction angle, φ (deg.)	0	0
wall friction, δ (deg.)	0	0

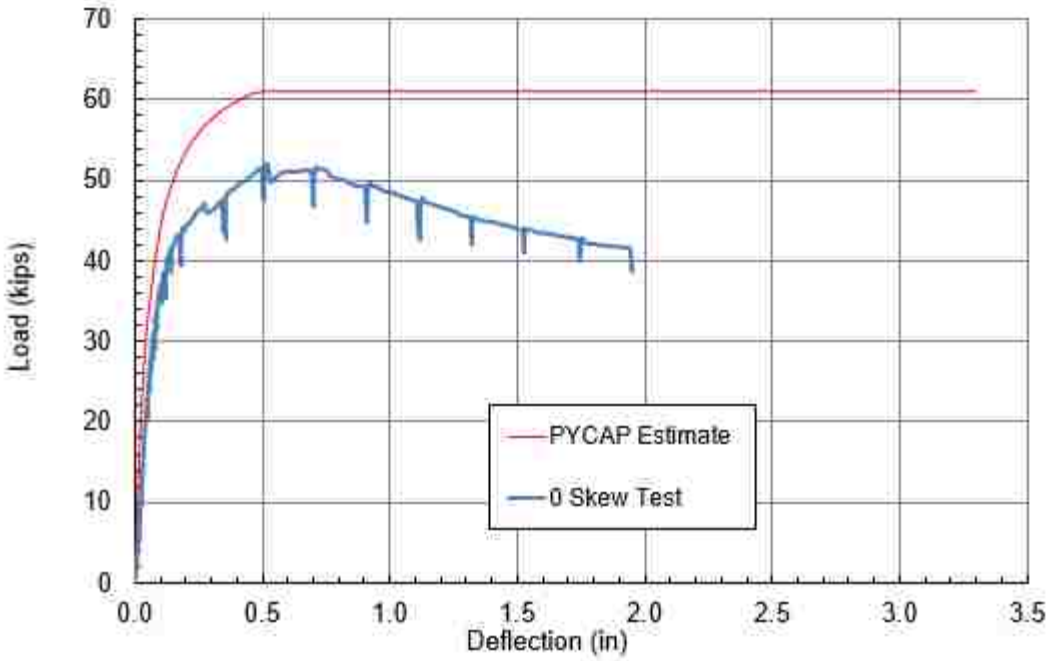

Figure 6-1: Comparison of measured passive force-deflection with curve computed by PYCAP for 0° skew test with φ=0 and c = 0.35UCS.

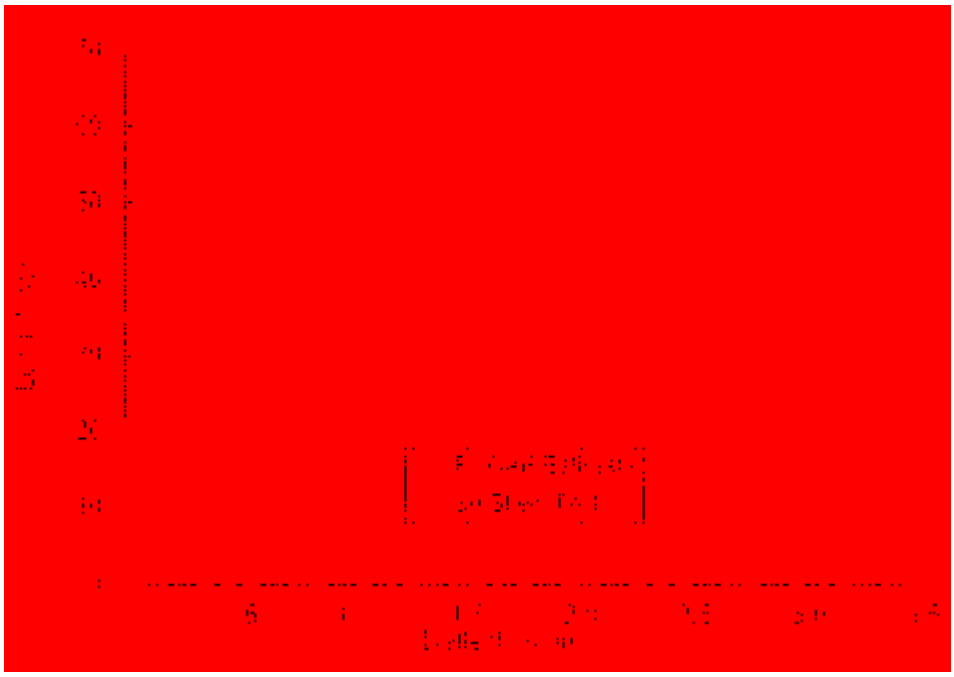

Figure 6-2: Comparison of measured passive force-deflection with curve computed by PYCAP for 30° skew test with φ=0 and c = 0.35UCS.

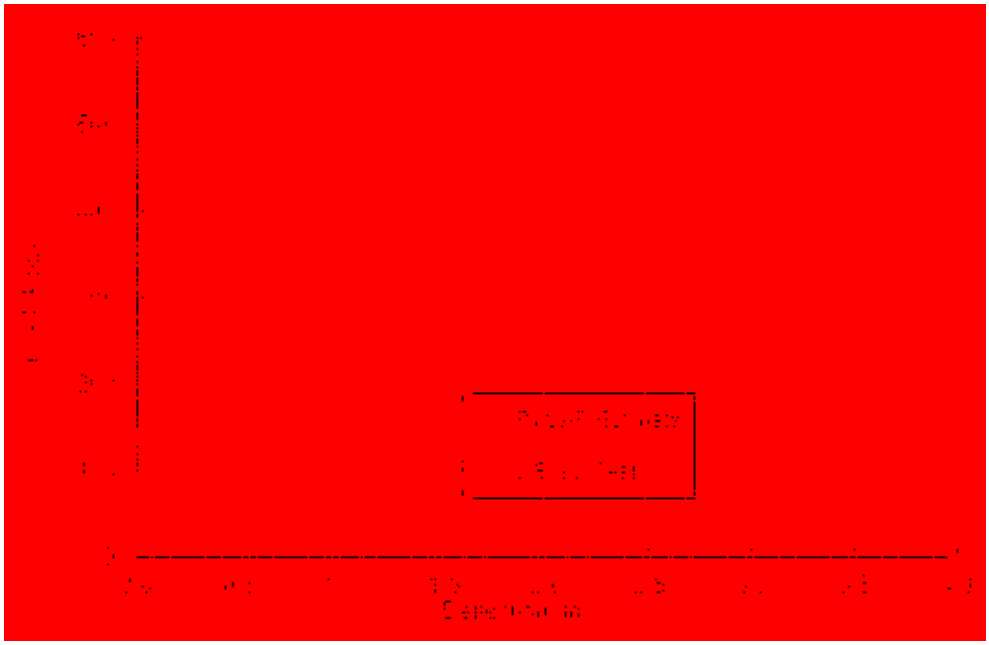

Figure 6-3: Comparison of measured passive force-deflection with curve computed by PYCAP for Remund (2017) 0° skew test with φ=0 and c = 0.35UCS.

6.3.2 PYCAP Analysis with Friction Angle to Match Observed Failure

A second analysis method using PYCAP was to use trial and error to input a friction angle until the predicted location of the surface failure was equal to the observed location of the surface failure from the test. This approach is illustrated in Figure 6-4. The surface failure for the 0° skew test was 7.25 feet and the surface failure for the 30° skew test was 8.17 feet. It is noted that for the 30º skew test the surface failure at the south end was used for calculation because the surface failure at the north end displayed a failure plane as predicted by the Rankine method.

The wall friction was calculated by multiplying the soil friction angle by a value of 0.67. Cohesion was lowered by trial and error until the PYCAP estimate was close to the observed values. The final input values shown in Table 6-4 were used to create Figure 6-5 and Figure 6-6.

Table 6-4: Final Trial and Error Friction Angle PYCAP Values

Input Parameters	0° Skew	30° Skew
cohesion, c (psf)	560	440
soil friction angle, φ (deg.)	37	40
wall friction, δ (deg.)	24.79	26.8

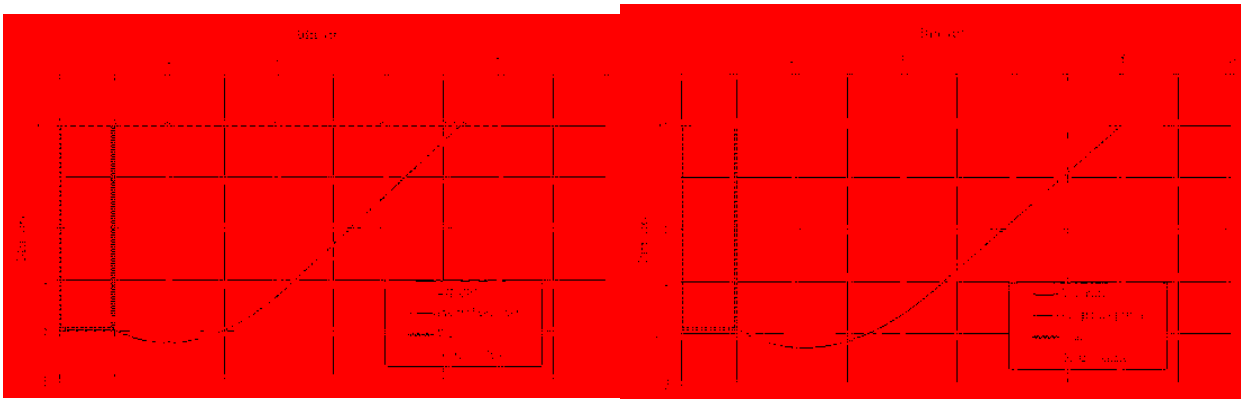

Figure 6-4: PYCAP log-spiral failure surfaces for the 0° skew (left) and 30° skew (right).

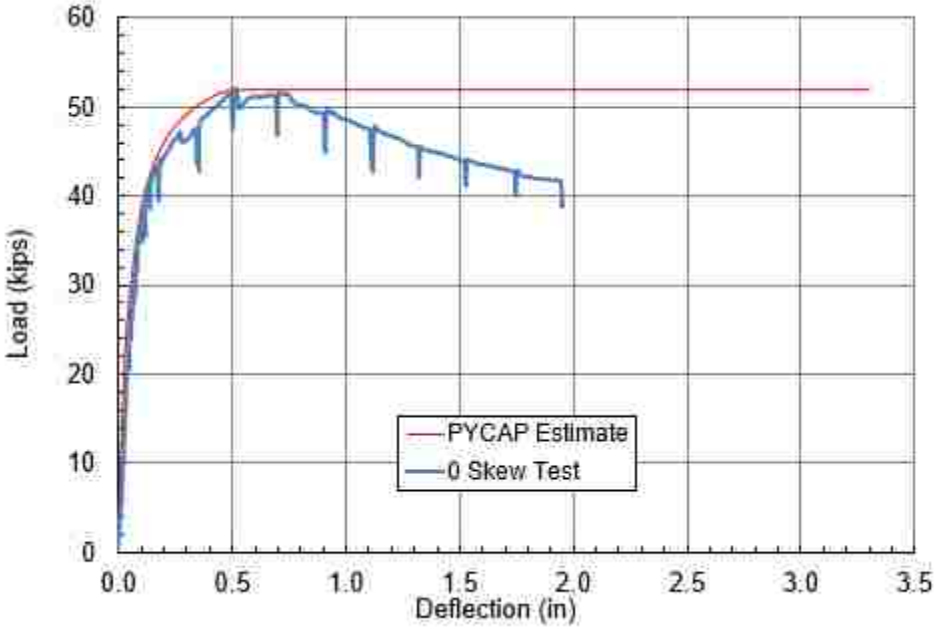

Figure 6-5: PYCAP analysis for 0° skew test with φ = 37° and c = 560 psf to match observed failure plane at surface of fill.

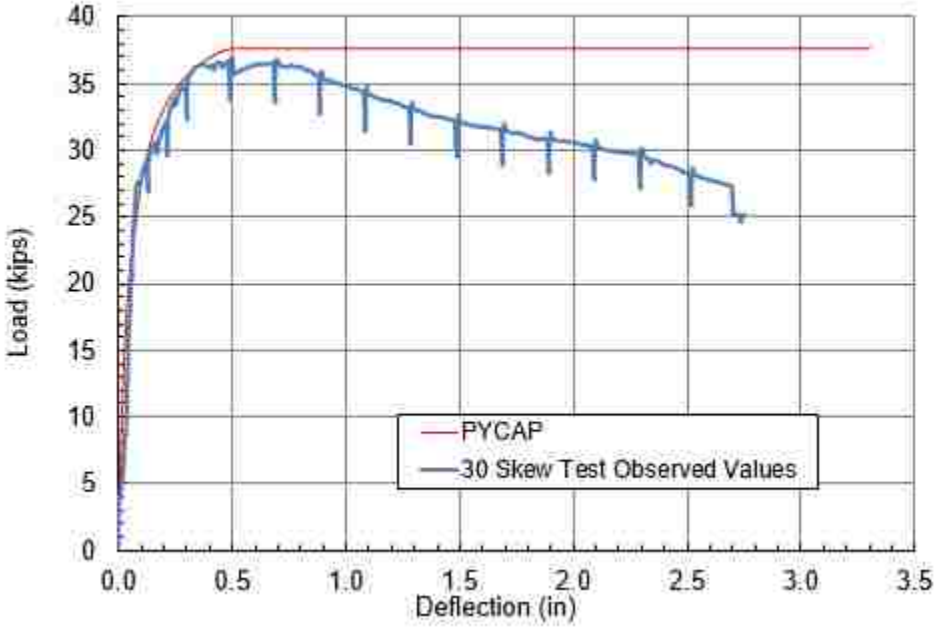

Figure 6-6: PYCAP analysis for 30° skew test with φ = 40° friction angle and c = 470 psf to match observed failure plane at surface of fill.

6.3.3 PYCAP Analysis with Recommended Friction Angle and Cohesion

A final method for using PYCAP to predict the passive force-deflection curve was to use the values suggested by Tiwari et al. (2017) of a friction angle of 35° and a corresponding cohesion of 36 kPa (750 psf) based on direct simple shear testing (DSS) or a friction angle of 34° and a corresponding cohesion of 78kPa (1630 psf) based on triaxial shear testing (CID). While the friction angles from these two tests are very similar (35° versus 34°), the cohesion values are very different (750 psf versus 1630 psf). If a friction angle of 34° is used without any cohesion, the computed passive force is only a small fraction of the measured resistance. This is because LCC has such a low unit weight that little friction is generated. Similarly, if the reported cohesion values are used in PYCAP with no friction angle, the computed force is again only a small fraction of measured resistance. Therefore, it is necessary to use an appropriate combination of both friction angle and cohesion to obtain the correct passive resistance.

The φ and c strength parameters proposed by Tiwari et al. (2017) were entered into PYCAP as shown in Table 6-5 and Table 6-6. Figure 6-7 and Figure 6-8 plot the measured passive force-deflection curves for the 0° skew test and the 30° skew test, respectively. The computed curves using the φ and c values obtained from the DSS and CID tests were also plotted to determine if the measured curves fall within the suggested range. The measured passive force-deflection curves for the 0° skew and 30° skew tests do not fall within the range of the two computed PYCAP curves. The computed curve obtained with the lower cohesion value provides the better agreement with the measured curves, generally speaking.

Table 6-5: PYCAP Recommended Input based on DSS Testing (Tiwari et al. 2017)

Input Parameters	0° Skew	30° Skew
cohesion, c (psf)	752	752
soil friction angle, f (deg.)	35	35
wall friction, d (deg.)	23.5	23.5

Table 6-6: PYCAP Recommended Input based on CID Testing (Tiwari et al. 2017)

Input Parameters	0° Skew	30° Skew
cohesion, c (psf)	1629	1629
soil friction angle, f (deg.)	34	34
wall friction, d (deg.)	22.8	22.8

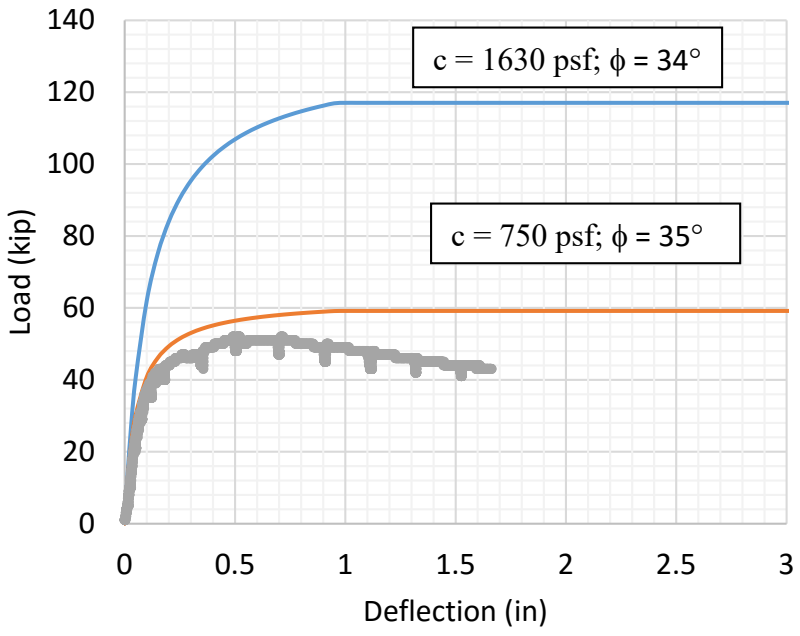

Figure 6-7: PYCAP analysis for 0° skew test with Tiwari et al. (2017) range.

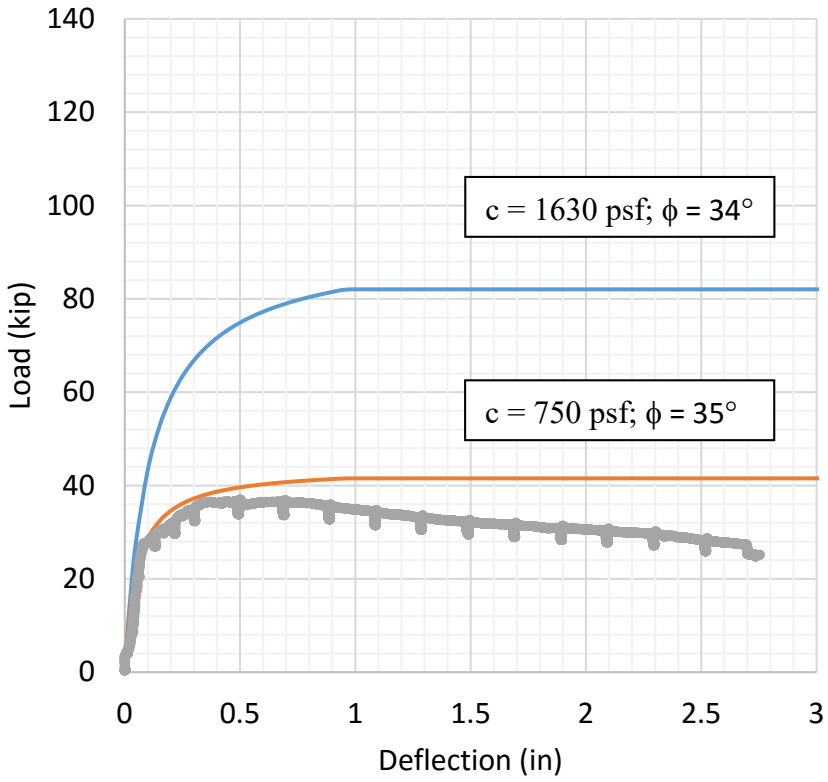

Figure 6-8: PYCAP analysis for 30° skew test with Tiwari et al. (2017) range.

6.3.4 PYCAP Analysis with φ = 34° and c = 700 psf

Slight modifications were made to the proposed range by Tiwari et al. (2017) to better fit the measured passive force-deflection curves. The friction angle of 34° was used because it agreed with the observed failure surface for the 30° skew test as determined by the equation proposed by Terzaghi and Peck (1948).

$$\alpha = 45 - \phi/2 \qquad \text{Equation 6-3}$$

where:

α = measured surface failure angle of 28° (see Section 5.4)

ϕ = 34°

The cohesion value was lowered to 700 psf to match both the 0° skew and the 30° skew measured passive force-deflection curves, as shown in Table 6-7. Figure 6-9 and Figure 6-10 plot the computed curve in comparison with the measured passive force-deflection curves for the 0° skew test and the 30° skew test, respectively. This method was also used to predict the passive force-deflection curve for the 0° skew LCC test performed by Remund (2017). As shown in Figure 6-11, the agreement between the measured and computed curves is quite good. Figure 6-12 compares the ranges for the cohesion values proposed by Tiwari et al. (2017) with the modified cohesion value used to obtain more accurate force-deflection curves for the LCC tests performed in this study. Figure 6-13 plots this cohesion intercept and friction angle Mohr envelope.

Table 6-7: PYCAP Input with φ = 34° and c = 700 psf

Input Parameters	0° Skew	30° Skew
cohesion, c (psf)	700	700
soil friction angle, φ (deg.)	34	34
wall friction, δ (deg.)	22.8	22.8

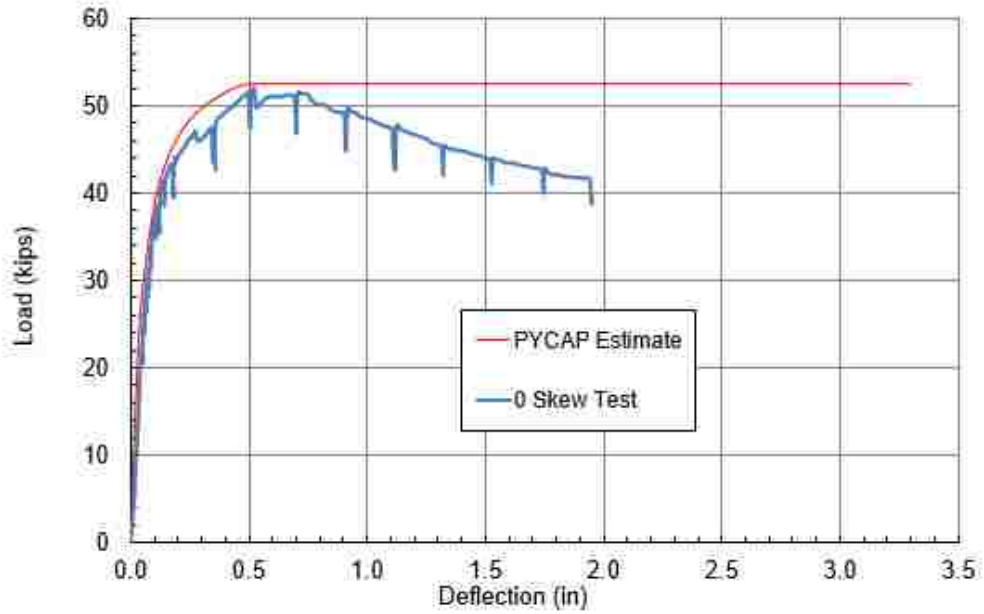

Figure 6-9: PYCAP analysis for 0° skew test with φ = 34° and c = 700 psf.

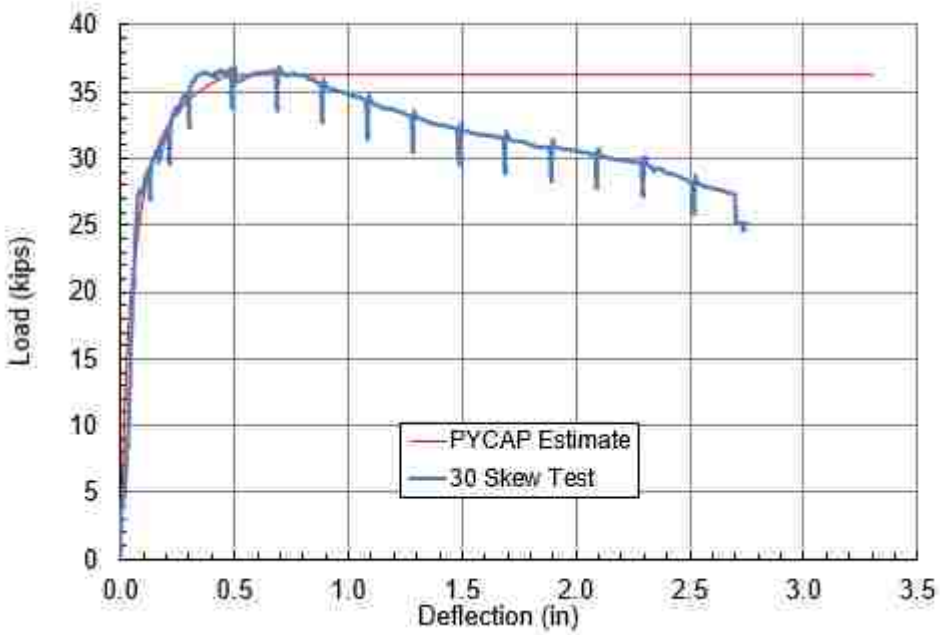

Figure 6-10: PYCAP analysis for 30° skew test with φ = 34° and c = 700 psf.

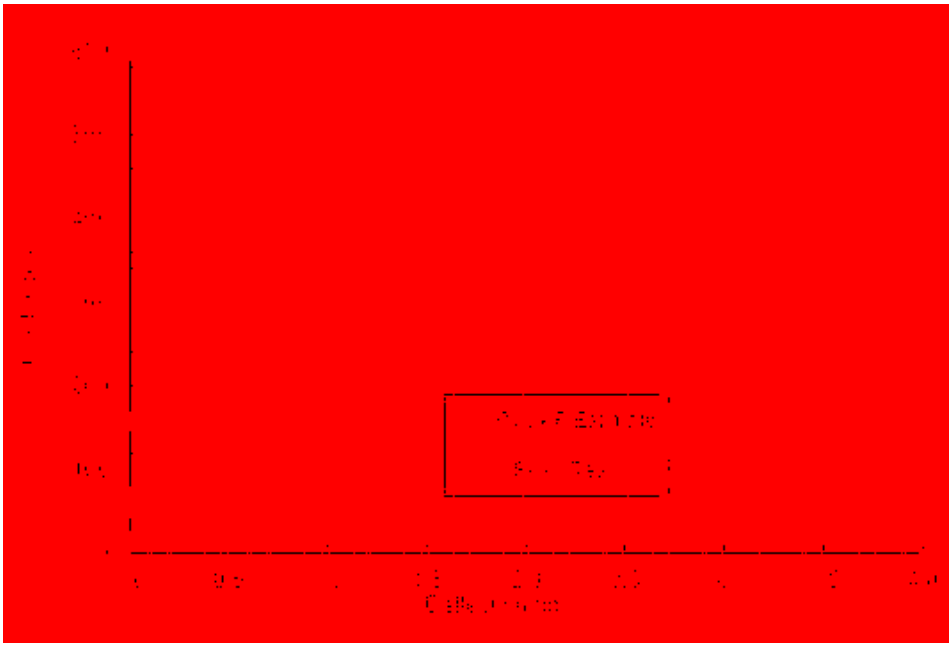

Figure 6-11: PYCAP analysis for Remund (2017) 0° skew test with φ = 34° and c = 700 psf.

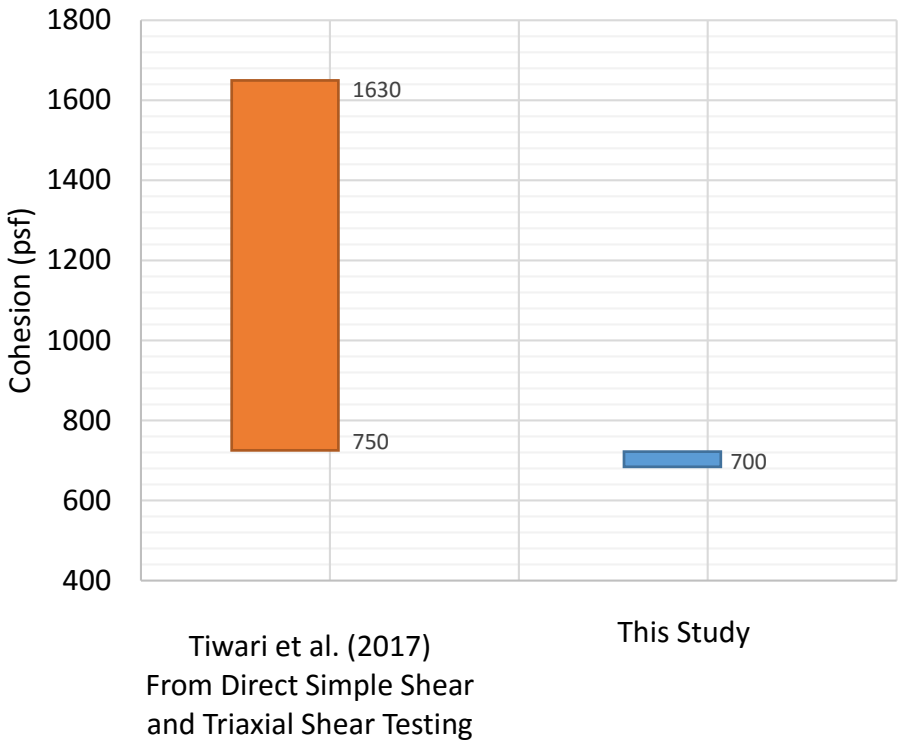

Figure 6-12: Cohesion value ranges for φ=34°-35°.

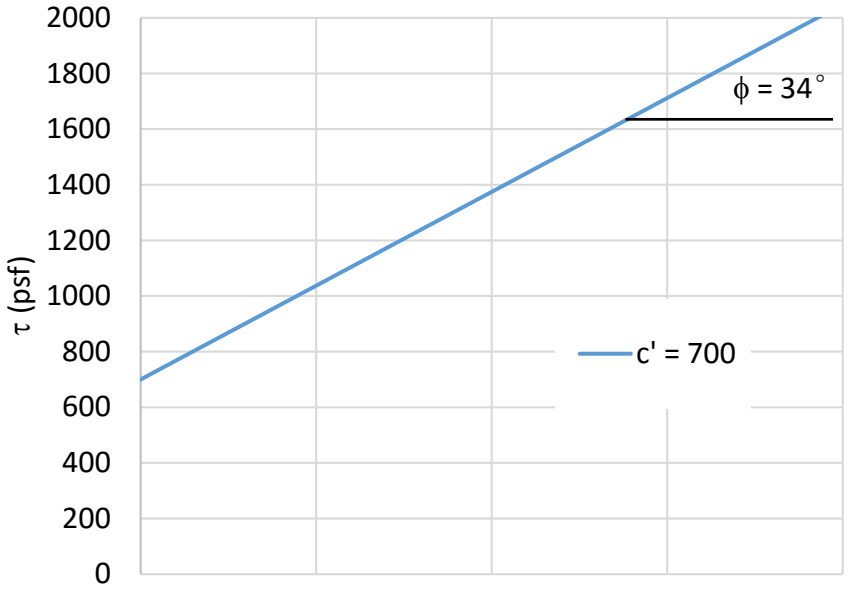

Figure 6-13: Cohesion intercept for φ = 34° and c = 700 psf.

6.3.5 PYCAP Analysis with φ = 34° and c = 0 psf

A proposed way to conservatively estimate peak passive resistance of LCC is to use a friction angle of 34° and a cohesion of 0. However, as shown in Figure 6-14, this only gives a resistance of about 2 kips. While Figure 6-14 only shows the results of the PYCAP analysis compared with the results of the 0° skew test, the results of the PYCAP analysis compared to the 30° skew test are similarly low. It is true that this is a conservative estimate, however, it is perhaps too conservative. Further testing of LCC material will determine if 700 psf is an accurate representation of cohesion, however, the data seems to indicate that including some amount of cohesion provides a more accurate prediction of peak passive resistance.

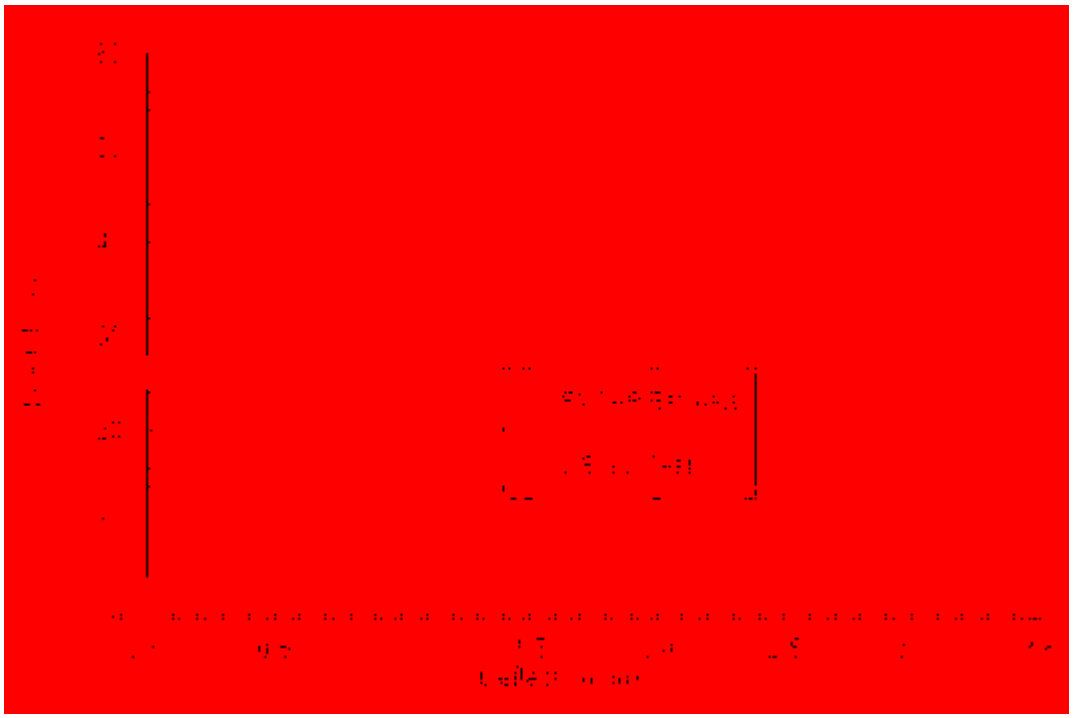

Figure 6-14: PYCAP analysis of 0° skew test with φ = 34° and c = 0 psf.

6.4 Granular Backfill Comparison

The Caltrans procedure for estimating passive resistance for granular backfill materials as reported by Remund (2017) is as follows:

$$K_{abut} = K_i * w * (h / 5.5\ ft) \quad \text{Equation 6-4}$$

where:

K_i = initial stiffness, approximately 50 kip/in/ft for embankment fill meeting Caltrans requirements and approximately 25 kip/in/ft for embankment fill not meeting Caltrans requirements

w = projected width of the backwall

h = height of the backwall

$$P_{bw} = A_e * 5.0\ ksf * (h_{bw} /5.5) \quad \text{Equation 6-5}$$

where:

A_e = effective abutment wall area

H_{bw} = height of backwall

This method appeared to have reasonable agreement with the large-scale tests performed by Remund (2017), however, because of the smaller scale of the tests performed for this study, the (h_w/5.5) factor led to an extremely low passive force-displacement curve estimation, as is shown in Figure 6-15. This could be used as an estimation but it would be extremely conservative in the case of smaller scale applications.

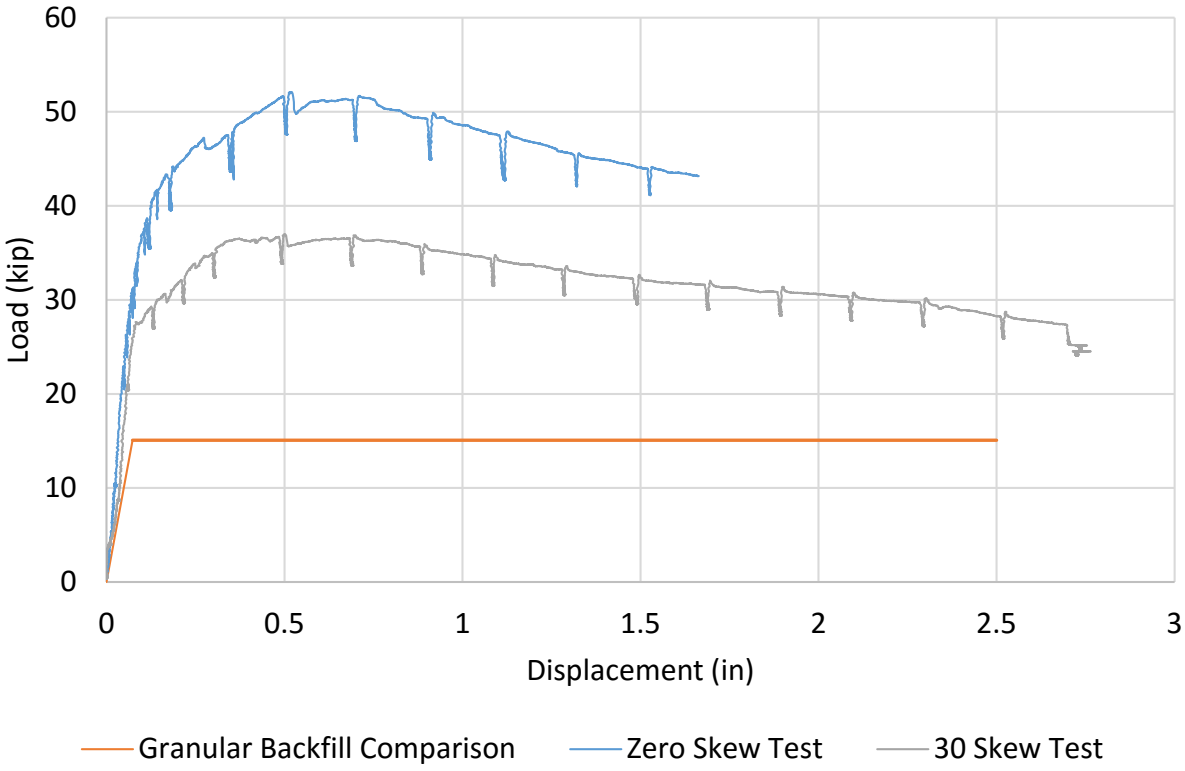

Figure 6-15: Comparison of passive force-deflection curve based on Caltrans equation for granular backfill relative to curves for 0° and 30° skew tests with LCC backfill.

7 CONCLUSIONS AND RECOMMENDATIONS

7.1 Conclusions

1.) In contrast to previous large-scale tests the backwall skew appeared to have a significant effect on the passive resistance of a cellular concrete backfill. The 30° skew produced a decrease in passive resistance of about 30%. This could indicate an R_{skew} value of 0.7 as opposed to the 0.5 for granular backfill.

2.) The displacement required to mobilize peak passive resistance of cellular concrete was 0.5 in, or 0.02 times the height of the backwall. This was consistent for both the 0° skew and the 30° skew tests, but is somewhat lower than the typical range of 0.03 to 0.05 times the backwall height for granular backfill.

3.) Initial stiffness of the passive force-deflection relationship for the cellular concrete at 0° skew angle was 76 kips/in per foot of wall width which is about twice as high as that measured in similar tests involving granular backfill.

4.) In contrast to the tests reported by Remund (2017), the cellular concrete did exhibit a decrease in passive force of about 15-20% after reaching a peak value. However, it was not a sudden nor large decrease in force. It behaved very similarly to the test of compacted sand performed by Rollins and Jessee (2013).

5.) It is not conclusive which method is preferable for predicting passive force-deflection curves relative to measured behavior. One method is to use a friction angle of 34 degrees

and a cohesion value of 700 psf. This method best fits the data of the two LCC tests, as well as the data for the 0° skew tests by Remund (2017). However, there are only three tests at present, therefore this conclusion is provisional at the moment. Another method is to use the Rankine equation as shown in Equation 6-1 and a reduction factor of 0.7 (corresponding to 0.35 times the unconfined compressive strength), although this method did not provide extremely accurate results for the observed test data. A final method is to use the program PYCAP with a friction angle of 0 and a cohesion equal to 0.7 times of 50% of the unconfined compressive strength. Once again, this method did not provide accurate results for the observed test data. Further research is needed to verify which of the proposed methods is the most consistently reliable.

7.2 Recommendations for Future Research

More definitive conclusions could be made about the decrease in passive resistance forces due to skew if there were more consistency in the backfill properties for the tests. It could perhaps be beneficial to build skew boxes side by side and do the pours on the same day. If that wasn't a possibility, it would be beneficial to ensure that the two batches of cellular concrete used for the large scale tests had more consistent wet densities. Although this is difficult to do, as cellular concrete becomes increasingly used the pump truck operators may be able to provide a more consistent wet density.

Another recommendation would be to perform the two passive force resistance tests after identical curing times. The large scale test for the 0° skew was done after six days of curing, while the large scale test for the 30° skew was done after five days of curing. This could have a small

effect on the peak passive resistance that was observed. Additionally, if the large-scale testing was done after a period of curing of 28 days, that may be a better measure of ultimate passive force.

Further research could also be done on the effect of other skew angles. A 15° skew test and a 45° skew test could provide further insights into the effect that skew has on peak passive force observed in cellular concrete. It would be most easily correlated to this study if similar test box dimensions and loading procedures were used, to limit external variables that could influence the results.

A final recommendation for future research is to do several tests with no skew, and take apart the test each time to evaluate the failure surface. In this test, the zero skew failure surface could only be extrapolated from the line of surface cracking. However, if the concrete exhibited a log-spiral form of failure then that would affect the angle used in other calculations. Additionally, further large scale tests could help determine which of the passive force prediction methods yields the most accurate results over multiple tests.

REFERENCES

ACI Committee 523. 2006. "Guide for Cast-in-Place Low Density Cellular Concrete."

Burke, M.P. Jr. 1994. "Semi-Integral bridges: movements and forces." *Transportation Research Record 1460* 1-7.

Clough, G.W, and J.M. Duncan. 1991. "Earth Pressures." *Foundation Engineering Handbook* 223-235.

Cole, R. T., Rollins, K. M. 2006. "Passive Earth Pressure Mobilization during Cyclic Loading." *Jounal of Geotechnical and Geoenvironmental Engineering* 1154-1164.

Duncan, J. Michael, and Robert L. Mokwa. 2001. "Passive Earth Pressures: Theories and Tests." *Journal of Geotechnical and Geoenvironmental Engineering* 248-257.

FHWA, NHI-15-004. 2014. "LRFD Seismic Analysis and Design of Bridges."

Filz, George, Alex Reeb, Alex Grenoble, and Farzad Abedzadeh. 2015. "Material Properties for Analysis of Deep Mixing Support Systems." *Deep Foundations Institute* 823-834.

Franke, B. W. 2013. *Passive Force on Skewed Abutments with Mechanically Stabilized Earth (MSE) Wingwalls Based on Large-Scale Tests.* Paper 3909, All Theses and Dissertations.

Fredrickson, A. 2015. *Large Scale Testing of Passive Force Behavior for Skewed Bridge Abutments with Gravel and Geosynthetic Reinforced Soil (GRS) Backfills.* Paper 5513, All Theses and Dissertations.

Grutzeck, Michael W. 2005. "Cellular Concrete." In *Cellular Ceramics: Structure, Manufacturing, Properties and Applications*, 193-223. Wiley-VCH Verlag GmbH & Co. KGaA.

Jessee, S. J. 2012. *Skew Effects on Passive Earth Pressures Basd on Large-Scale Tests.* All Theses and Dissertations.

LaVallee, Steve. 1999. *Cellular concrete to the rescue.* Boston: The Aberdeen Group.

Lee, K.L., and A. Singh. 1971. "Relative Density and Relative Compaction." *J. Soil Mech and Found. Div.* 1049-1052.

Mokwa, Robert L., J. Michael Duncan, and Charles E. Via. 2000. *Investigation of the Resistance of the Pile Caps and Integral Abutments to Lateral Loading.* Charlottesville, VA: Virginia Transportation Research Council.

Nambiar, E. K. Kunhanandan, and K. Ramamurthy. 2009. "Shrinkage Behavior of Foam Concrete." *Journal of Materials in Civil Engineering* 631-636.

Ramamurthy, K., and E.K. Kunhanandan Nambiar. 2009. "A classification of studies on properties of foam concrete." *Cement & Concrete Composits* 388-396.

Remund, Tyler. 2017. "Large-Scale Testing of Low-Strength Cellular Concrete for Skewed Bridge Abutments." *All Theses and Dissertations* (All theses and disertations).

Rollins, K. M, A.S. 2002. "Lateral Resistance of Full-Scale Pile Cap with Gravel Backfill." *Eng. Journal of Geotechnical and Geoenvironmental Engineering* 711-723.

Rollins, K. M., and A. Sparks. 2002. "Lateral Resistance of full-scale pile cap with gravel backfill." *Journal of geotechnical and geoenvironmental engineering* 711-723.

Rollins, Kyle M., and Shon J. Jessee. 2013. "Passive Force-Deflection Curves for Skewed Abutments." *Journal of Bridge Engineering* 1086-1094.

Shamsabadi, A, M Kapuskar, and A Zand. 2006. *Three-dimensional nonlinear finite-element soil-abutment structure interation model for skewed bridges.* 5th National Seismic Conf. on Bridges and Highways, FHWA.

Shamsabadi, Anoosh, Kyle M. Rollins, and Mike Kapuskar. 2007. "Nonlinear Soil-Abutment-Bridge Structure Interaction for Seismic Performance-Based Design." *Journal of Geotechnical and Geoenvironmental Engineering* 707-720.

Shamsabadi, Anooshirvan. 2006. *Three-Dimensional Nonlinear Seismic Soil-abutment-foundation-structure Interaction Analysis of Skewed Bridges.* Dissertation, University of Southern California.

Sutmoller, Nico. 2017. *An Introduction to Cellular Concrete and Andvanced Engineered Foam Technology.* Presentation, Aerix Industries.

Taylor, Scott M. 2014. "Cellular Concrete." *Structure Magazine* 41-44.

Terzaghi, Karl, and Ralph B. Peck. 1948. *Soil Mechanics in Engineering Practice.*

Tiwari, Binod, Beena Ajmera, and Diego Villegas. 2018. "Dynamic Properties of Lightweight Cellular Concrete for Geotechnical Applications." *Journal of Materials in Civil Engineering.*

Tiwari, Binod, Beena Ajmera, Ryan Maw, Ryan Cole, Diego Villegas, and Peter Palmerson. 2017. "Mechanical Properties of Lightweight Cellular Concrete for Geotechnical Applications." *Journal of Materials in Civil Engineering* 1-7.

Ulm, France-Josef, Hamlin M. Jennings, and Roland Pellenq. 2013. *Mechanics and Physics of Creep, Shrinkage, and Durability of Concrete.* American Society of Civil Engineers.

Wagstaff, Kevin Bjorn. 2016. "Evaluation of Passive Force on Skewed Bridge Abutments with Controlled Low-Strength Material Backfill." *All Theses and Dissertations* 5824.